NASA CONTRACTOR REPORT

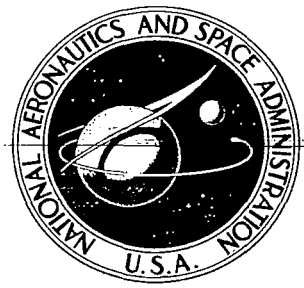

NASA CR-1333

A THEORY FOR PREDICTING THE ROTATIONAL AND VORTEX NOISE OF LIFTING ROTORS IN HOVER AND FORWARD FLIGHT

by S. Gene Sadler and Robert G. Loewy

Prepared by
ROCHESTER APPLIED SCIENCE ASSOCIATES, INC.
Rochester, N. Y.
for Langley Research Center

NATIONAL AERONAUTICS AND SPACE ADMINISTRATION • WASHINGTON, D. C. • MAY 1969

NASA CR-1333

A THEORY FOR PREDICTING THE ROTATIONAL AND VORTEX NOISE OF LIFTING ROTORS IN HOVER AND FORWARD FLIGHT

By S. Gene Sadler and Robert G. Loewy

Issued by Originator as RASA Report No. 68-11

Prepared under Contract No. NAS 1-7618 by
ROCHESTER APPLIED SCIENCE ASSOCIATES, INC.
Rochester, N.Y.

for Langley Research Center

NATIONAL AERONAUTICS AND SPACE ADMINISTRATION

For sale by the Clearinghouse for Federal Scientific and Technical Information
Springfield, Virginia 22151 – CFSTI price $3.00

CONTENTS

A THEORY FOR PREDICTING THE ROTATIONAL AND VORTEX NOISE OF LIFTING ROTORS IN HOVER AND FORWARD FLIGHT

By S. Gene Sadler and Robert G. Loewy

SUMMARY

In the analysis techniques developed in this report the lifting rotor was considered as a swept surface on which area segments are subjected to oscillating pressures expressed as a Fourier series in time. The oscillating pressures were assumed to be separable into those giving rise to normal lift and drag, i.e., associated with resultant angle of attack changes (rotational effects), and those associated with the shedding of eddies as a result of boundary layer oscillations on bluff bodies (vortex street effects). The sound pressure at any field point was then found by numerical integration over all the area segments of the swept surface.

This method allows either near or far field noise to be calculated, including all effects other than blade thickness and random turbulence in the boundary layer or the wake. The effects of both impulsive changes in load around the azimuth and that of vortex noise were investigated for various flight conditions for the H-34 helicopter and for the HU-1A helicopter in hover. The predicted noise is presented both as plots of sound pressure level versus harmonic number and by plots of pressure time history. Comparisons of predicted results with appropriate measurements obtained for the HU-1A and H-34 were made for selected cases.

The main overall results of the investigation were that the inclusion of vortex shedding effects in addition to the rotational effects significantly improved the prediction of the measured noise levels as compared to that obtained by considering only rotational effects, and that "blade slap" characteristics are most readily observed and thus investigated through the use of pressure time history plots.

INTRODUCTION

The use of turbine power plants in rotary wing and V/STOL aircraft leaves the rotor-propeller as an important source of low-frequency noise. Military applications of helicopters in tactical situations (ref. 1), as well as increased commercial use in heavily

populated areas, have made understanding the lifting rotor-propeller as a noise source an important technical objective. Discomfort, proficiency impairment, and the danger of permanent hearing loss due to high intensity noise inside the aircraft are important additional motivations for developing better understanding of rotor noise. This is especially true since it is generally accepted (see ref. 2, for example) that reductions of low frequency noise inside the aircraft must be achieved at the source. In particular, the weight penalty for significant attenuation inside the aircraft is usually prohibitive for frequencies below about 200 cps. It is apparent therefore that if the required reductions are to be obtained by modification of the basic elements which produce the noise these characteristics must be fully understood before they can be successfully modified.

A considerable foundation of experience that can be applied to the subject problem exists by virtue of propeller noise research performed in the past (ref. 3, 4 and 5). In addition, several programs directed at increasing the understanding of rotor noise have been carried out recently (ref. 6 through 10). Nevertheless, successful prediction of the sound pressure level versus frequency has not been realized to date. It is believed that previous attempts have not been successful because both the rotational and the vortex shedding effects have not been considered simultaneously in the development of these methods. Acceptable prediction of the sound pressure level versus frequency is important to provide the understanding that is required before any investigation to reduce the noise level can be successfully accomplished. The purpose of the present study, therefore, was to develop a method by which both the rotational and vortex shedding effects are properly accounted for in the prediction of the noise generated by a lifting rotor.

Garrick and Watkins' work (ref. 5) and extensions of it have dealt with rotational noise generated by propellers. In reference 9 the theory of Garrick & Watkins was extended to allow prediction of the rotational noise generated by lifting rotors in forward flight. This theory for predicting helicopter rotor noise has been extended here to include the effects of the rotor being acted upon by lift and drag forces associated with vortex street type of shed vorticity as described by Yudin (ref. 11).

The authors wish to acknowledge the assistance of Mr. Harry Sternfeld and Mr. Robert Spencer of The Vertol Division of The Boeing Company, who provided narrow band sound spectrum analyses and pressure time histories for use in the comparison of theoretical and measured data.

SYMBOLS

a, d, f, g, l	pulse shape variables, see Fig. 9, dimensionless
a_{m_i} , b_{m_i}	normalized Fourier coefficients of general pressure pulse, dimensionless
ASL	aerodynamic section loading, i.e. force normal to the blade chord per unit span, pounds/inch
B	number of rotor blades
c	wave speed, feet/second
C	velocity of sound, feet/second
C_i	blade chord at $i^{\underline{th}}$ radial station, feet
$C_i' = C_i \cos \theta_i$	steady part of the projection of blade chord on the plane perpendicular to the shaft, feet
$C_{L_{ij}}$, $C_{D_{C_{ij}}}$, $C_{D_{W_{ij}}}$, $C_{D_{ij}}$	coefficients of lift, incompressible drag, compressibility drag, total drag, respectively at source point ij, dimensionless
$C_{LV_{ij}}$, $C_{DV_{ij}}$	coefficients of oscillatory lift and drag at source point ij, dimensionless
(C_{m_i}, ψ_{m_i}), (d_{m_i}, Γ_{m_i}) (e_{m_i}, K_{m_i})	amplitude coefficients of Fourier series for lift, incompressible drag, compressibility drag, respectively at radius station i, dimensionless
$(CV_{m_{ij}}, \psi V_{m_{ij}})$ $(dV_{m_{ij}}, \Gamma V_{m_{ij}})$	amplitude coefficients of Fourier series for vortex street lift and drag, respectively at source point ij, dimensionless
d	projected body dimension in a direction perpendicular to the local resultant velocity, feet
e	flapping hinge offset, feet

f	frequency of vortex street shedding, cycles per second
$F_{m_{x_{ij}}}$, $F_{m_{y_{ij}}}$, $F_{m_{z_{ij}}}$	complex amplitude of force acting on the fluid in the x, y, z directions, respectively, at the frequency of the $m^{\underline{th}}$ harmonic, at the source point ij
h	vertical distance between rows of vortices in the vortex street, feet
$i = \sqrt{-1}$	imaginary unit
$k_m = \frac{mB}{C}$	inverse of wave length of $m^{\underline{th}}$ harmonic, 1/feet
L_{ij}, $D_{c_{ij}}$, $D_{w_{ij}}$, D_{ij}	lift, incompressible drag, compressible drag, total drag, respectively, acting on incremental span length at source point ij, pound/foot
$L_{v_{ij}}$, $D_{v_{ij}}$	oscillatory lift and drag acting on incremental span length at source point ij, pound/foot
m	harmonic number
$M_N = V/C$	Mach number
$M_{N_{ij}} = V_{ij}/C$	Mach number of a blade element at source point ij
n	number of azimuthal increments
P	sinusoidally varying pressure, dynes/cm^2
P_ω, P_m	complex amplitude of pressure sinusoidally varying at frequency ω or harmonic m
q	blade twist angle over blade length from flap hinge to tip, positive when decreasing with increasing radius, radians
r_i	blade radius at station i, measured from shaft axis along unflapped blade, feet
R	total rotor radius, feet

$S_R = \frac{fU_b}{h}$ Roshko's "universal Strouhal number"

$S_t = \frac{fU}{d}$ Strouhal number

$SPL = 20 \log_{10} \frac{P_{rms}}{P_{ref}}$ sound pressure level, decibels

t time, sec, measured from $\psi = 0$

$T = \frac{2\pi}{B\Omega}$ fundamental period, second

U_b velocity just outside boundary layer, at separation point of wake, feet/second

U_{ij} resultant air velocity perpendicular to a blade leading edge at source point ij, feet/second

U_p component of U_{ij} perpendicular to plane perpendicular to shaft axis swept surface, positive up, feet/second

U_T component of U_{ij} tangent to a plane perpendicular to the shaft axis, feet/second

V aircraft forward velocity, feet/second

V_D aircraft descent velocity, feet/second

α_{ij} blade element aerodynamic angle of attack at source point ij, radians

α_s tilt of rotor shaft relative to vertical, positive aft, radians

β_0 coning angle, measured positive up from a plane perpendicular to the shaft arm, radians

β_1 coefficient of longitudinal flapping, positive so as to make rotor shaft tilt aft, radians

β_2 coefficient of lateral flapping, positive so as to make rotor shaft tilt to port, radians

$\gamma = \sqrt{1 - M_N^2}$

Γ	circulation of an individual vortex in the vortex street, feet^2/second
$\theta_1 = \theta_0 - \frac{q(r_i-e)}{(R-e)}$	steady part of θ_{ij}, radians
θ_0	collective geometric pitch angle, radians, positive nose up
θ_1	lateral cyclic pitch angle, radians, positive nose up
θ_2	longitudinal cyclic pitch angle, radians, positive nose up
ρ	air mass density, slugs/feet^3
$\tau_{ij} = \frac{c_i \cos \theta_{ij}}{r_i}$	duration of pressure pulse at source point ij, second
ψ	azimuth angle zero in the trailed position, degrees or radians
$\theta_{ij} = \alpha_{ij} - \theta_{ij}$	non-geometric part of angle of attack at source point ij, radians
$= \arctan (U_p/U_T)_{ij}$	
ω	frequency of oscillatory pressure, radians/second
Ω	rotor angular velocity, radians/second

Subscripts

i	radial station
I	imaginary part
j	azimuthal station
m	harmonic number
o	field point, or steady component
R	real part
x, y, z	direction of force, along positive Cartesian axes
ω	frequency component

ANALYSIS

The formulation of the technique developed herein follows the general procedure developed in reference 9. The effects of the approximately "white" noise which exists in the turbulent boundary layer sheathing the blades, which is modulated for the observer at the blade passage frequency (ref. 7) was ignored in this study. Also, as discussed in references 12 and 13, pressure fluctuations due to the passage of the complex wake of trailed vorticity as experienced by an observer translating with the rotor were not considered. The effects of the trailed vorticity were accounted for indirectly through their effect on the azimuthal and radial distribution of the blade loads. Effects specifically accounted for in the analysis procedure developed herein include:

1. azimuthal and radial variations of the velocity normal to the leading edge, the angle of attack, and the lift and drag forces;

2. non-linear and compressible airfoil section characteristics;

3. numerical integration over the rotor, eliminating near and far-field approximations;

4. reversed flow;

5. blade coning, collective pitch, and first harmonic flapping and cyclic pitch; and

6. azimuthal and radial variations of the vortex street shedding frequency and strength.

The effects of radial and azimuthal inflow nonuniformities at the rotor whether due to the fundamental aerodynamic characteristics of rotors in forward flight or due to blade-fuselage and/or rotor-rotor interference were, of course, included in that the method uses measured blade air loads.

A numerical approach to the prediction of the rotational noise has been shown to be useful (ref. 9) in that the previously discussed effects can be included to any desired degree of refinement. For this reason, the same approach has been used in the development of the method reported herein, which includes both rotational and shed vortex effects. Since the method formulated herein makes use of Garrick and Watkins' basic theory (ref. 5) the distortion of dipole radiation pattern and Doppler effects (which can cause significant frequency shifts for an observer in the nonrotating system) are an inherent part of the analysis procedure.

Derivation of Acoustic and Geometric Relationships

Three coordinate systems were used in the analysis technique that is developed herein. A polar coordinate system was used to describe the azimuthal and radial variation of blade forces in the rotor disc, the Cartesian coordinate system was used to describe the location of a source point on the disc with respect to an observer, and a polar coordinate system was used to describe the location of an observer. All of the coordinate systems have their origin at the center of the rotor hub (see figure 1), so that they translate with the flight velocity, V. The Cartesian coordinate system is oriented such that (1) the z-axis is vertical, and (2) the positive x-direction points in the direction of flight. The polar coordinate system which describes the location of an observer measures the azimuth angle, ψ_0, in the x-y plane and is zero on the negative x-axis. The polar coordinate system which describes the location of quantities in the rotor disc is oriented such that the azimuth angle, ψ, is defined in a plane perpendicular to the shaft and is taken to be zero on the negative x-axis, as is shown in figure 2. Points on the surface area swept out by the rotor blades at which the instantaneous blade forces are assumed to act are called "source points" and are located by x, y, z coordinates. A general point outside the swept area but translating with the rotor is called a "field point" and is located by x_0, y_0, z_0 in the Cartesian coordinate system and by R_0, ψ_0, Z_0 in a polar coordinate system. Since integration is performed over the swept area, the "source points" are specified using a double subscript notation i, j. Here i identifies the radial position and j the azimuthal position.

Equations for determining x, y, z coordinates of the source points are derived geometrically by examining the position of a particular blade of the rotor at any time, t. It was assumed that the blade is inflexible but has a "flapping hinge," offset a distance, e, from the center of rotation. This allows a blade to rotate out of the plane of rotation through an angle β_j, which is assumed to be small. A point on the blade is defined as being a distance r from the center of rotation when $\beta = 0$. No other motion of the blades with respect to the hub, other than pitch changes (denoted by θ_{ij}), were taken into account. The rotor shaft is allowed to be tilted through an angle α_s in the longitudinal plane. Blade point coordinates are then given (see, for example, ref. 14), when small angle assumptions are made for sin β and cos β, by

$$x_{ij} = - r_i \cos \psi_j \cos \alpha_s - \beta_j (r_i - e) \sin \alpha_s \qquad (1a)$$

$$y_{ij} = - r_i \sin \psi_j \tag{1b}$$

$$z_{ij} = - r_i \cos \psi_j \sin \alpha_s + \beta_j (r_i - e) \cos \alpha_s \tag{1c}$$

As in reference 5, the sinusoidally varying pressure at a field point (x_0, y_0, z_0) with the frequency $\omega = mB\Omega$ is defined as

$$P(x_0,y_0,z_0,t) = \mathrm{Re}\left[P_\omega(x_0,y_0,z_0)e^{i\omega t}\right] = \mathrm{Re}\left[P_m(x_0,y_0,z_0)e^{imB\Omega t}\right] .$$

Here Ω is the rotating frequency of the rotor, and Re, of course, signifies taking the real part of a complex number. Periodic conditions are assumed; i.e., what happens in one revolution happens in every other, and in fact, what happens to one blade at a particular azimuth is repeated on every other blade when it is at that azimuth. It follows, therefore, that the fundamental period is $T = \frac{2\pi}{\Omega B}$; and m is the harmonic number. By determining the harmonic components of the forces acting on the fluid at a source point in the directions of the coordinate axes, namely $F_{m_{x_{ij}}}$, $F_{m_{y_{ij}}}$, and $F_{m_{z_{ij}}}$, then the sound pressure at a field point can be calculated from the expression

$$\mathrm{Re}\left[P_m(x_0,y_0,z_0)e^{imB\Omega t}\right]$$

$$= \mathrm{Re}\left[\frac{1}{4\pi}\left(F_{m_x}\frac{\partial}{\partial x_0} + F_{m_y}\frac{\partial}{\partial y_0} + F_{m_z}\frac{\partial}{\partial z_0}\right)\frac{e^{-ik\sigma}}{S}\, e^{imB\Omega t}\right] \tag{2}$$

which was given, in slightly different form, as eq. (6) in reference 5. Here,

$$k = \frac{mB}{C}$$

$$S = \sqrt{(x_0 - x)^2 + \gamma\left[(y_0 - y)^2 + (z_0 - z)^2\right]}$$

$$\sigma = \frac{M_N(x_0 - x) + S}{\gamma^2}$$

$$M_N = \frac{V}{C}$$

C = velocity of sound

$$\gamma = \sqrt{1 - M_N^2} \qquad (2a)$$

As may be seen from equation (2), Fourier components of force vectors are needed for computation of sound pressures. In order to compute these forces, however, the blade normal and tangential velocity components and the angle of attack must be determined.

The normal velocity component designated by U_p is parallel to the shaft axis and is positive up, and the tangential velocity component U_T, is perpendicular to the shaft axis and is positive when directed toward the airfoil leading edge. Accounting for components of forward speed, rotational speed, descent speed, an average induced velocity component v, (assumed positive down) and an effective component normal to the chord as a result of flapping velocity $\dot{\beta}$, yields the following expressions for the two velocity components,

$$U_T = V \cos \alpha_s \sin \psi + \Omega r - V_D \sin \alpha_s \sin \psi,$$

$$U_p = V (\sin \alpha_s - \beta \cos \alpha_s \cos \psi) - v - \dot{\beta}(r - e) + V_D \cos \alpha_s.$$

These expressions for the velocity components were derived neglecting the radial component of velocity, applying the small angle approximation to the flapping motion, and assuming that the usual two-dimensional strip theory approach is applicable. The actual induced velocity is a quantity, which, in general, varies both over the blade radius and azimuth, and its calculation has been the subject of extensive research. Its effect on angle of attack may be quite significant, especially where U_p might otherwise be small. It is usually assumed, however, that induced velocities in

the plane of the rotor are small compared to U_T, except where that velocity is small, in which case the resulting forces are unimportant. For this reason, the resulting velocity U_{ij} is calculated using an induced velocity v assumed to be uniform over the disc, and calculated for hover and forward flight from the momentum theory expression (ref. 15),

$$v = \frac{\text{thrust}}{2\pi R^2 \rho [(v \sin \alpha_s - v)^2 + (V \cos \alpha_s)^2]^{1/2}} .$$

For the case of a helicopter in vertical descent the induced velocity was determined approximately from figure 6 - 9 of reference 14.

As shown in figure 3, the blade angle of attack, α_{ij} is a function of the velocity components U_p and U_T and the local geometric blade pitch angle, θ_{ij}. As in reference 9, these velocity components are used in conjunction with experimentally determined airfoil section coefficients and measured aerodynamic normal forces to determine the radial and azimuthal variations of the section angle of attack and the lift and drag forces. The manner in which this is accomplished is presented in detail in reference 9 and is outlined briefly below. The resultant velocity for each element of swept area corresponding to a source point is calculated from

$$U_{ij} = \sqrt{U_p^2 + U_T^2}$$

$$= [(V \cos \alpha_s \sin \psi + \Omega r - V_D \sin \alpha_s \sin \psi)^2$$

$$+ (V \sin \alpha_s - V\beta \cos \alpha_s \cos \psi - v - \dot{\beta}(r - e) + V_D \cos \alpha_s)^2]^{\frac{1}{2}}$$

the Mach number from

$$M_{N_{ij}} = U_{ij}/C$$

and the normal force coefficient, $C_{N_{ij}}$, from

$$C_{N_{ij}} = \frac{(ASL)_{ij}}{1/2\rho(U_{ij})^2 c_i} \tag{3}$$

(Eq. 5 of ref. 9 has an error in this equation. The Δr_i term in the denominator of the right hand side should not have been present). These values for $M_{N_{ij}}$ and $C_{N_{ij}}$ were used to determine aerodynamic angle of attack, α_{ij}, coefficients of lift $c_{L_{ij}}$, incompressible drag, $c_{D_{v_{ij}}}$, and compressible drag, $c_{D_{w_{ij}}}$, from measured data. The details of this procedure are given in reference 9.

This method uses the sectional data to determine the aerodynamic forces acting on the blade as vectors parallel to and perpendicular to the instantaneous resultant velocity. It follows from a straightforward transformation of coordinates, using the approximations $\cos\beta \simeq 1$ and $\sin\beta \simeq \beta$, that the forces in the x, y, and z directions are

$$\begin{aligned}
F_x &= [(L\sin\phi - D\cos\phi)\cos\alpha_s \sin\psi \\
&\quad + (L\cos\phi + D\sin\phi)(\beta\cos\alpha_s\cos\psi - \sin\alpha_s) \\
F_y &= [(L\cos\phi + D\sin\phi)\beta\sin\psi - (L\sin\phi - D\cos\phi)\cos\psi] \\
F_z &= [(L\sin\phi - D\cos\phi)\sin\alpha_s \sin\psi \\
&\quad + (L\cos\phi + D\sin\phi)(\beta\sin\alpha_s\cos\psi + \cos\alpha_s)
\end{aligned} \tag{4}$$

respectively, where, for convenience, the subscripts m, i, and j are omitted and considered to be understood.

Representation of Vortex Street Characteristics

The vortex street phenomenon exists only when a separated wake exists, and viscous effects as seen in the boundary layer are the source of the wake. One of the objects of airfoil design is, of course, to minimize separation. It cannot be completely prevented, but in the normal operating range of angles of attack of smooth airfoils it occurs near the trailing edge. There is a dearth of references in the literature concerning vortex streets associated with airfoil shapes at angles of attack below stall. Some evidence that it does exist, as has been implicitly assumed by Yudin (ref. 13), Hubbard and Regier (ref. 18), and Schlegel, et al. (ref. 8), can be found. For example, Stowell and Deming (ref. 19) could not find a discrete vortex noise frequency during experiments in which all sections but one of a rotating rod were streamlined cross sections. This suggests strongly that the streamlined sections shed vortices as well as the non-streamlined section. As another instance, measurements of axial-flow fan noise showed a velocity dependency proportional to the sixth power of the tip speed (ref. 20). This result correlates well with the tip speed power dependence predicted by Yudin's theory, which is based on the vortex street mechanism. Also, Blokhintsev (ref. 21) reports that the vortex noise of propellers has a spectrum in which a narrow range of frequencies stands out relatively strongly, which is understandable if the intensity of the vortex noise is proportional to the sixth power of the velocity. These cases support the intuition of the earlier investigators (refs. 8, 13, and 18); namely, that the wake formed from a separated boundary layer might be influenced by its width at the separation point and the flow conditions there, but not by the detailed shape of the generating body.

Roshko (ref. 22) has shown from theory and experiment that the distance between the separation points on a bluff cylinder and the value of the pressure coefficient there determines the frequency of the vortex street and the width of the vortex street after the rows of the vortices become parallel. This clarifies the observed variation of Strouhal number with Reynolds number for a given body. The Strouhal number had been defined as

$$S_t = \frac{fU}{d}$$

where S_t = Strouhal number

d = projected dimension of the body perpendicular to the resultant velocity

U = resultant velocity, and

f = vortex street shedding frequency, in cycles per second.

The Strouhal number defined by this relationship, however, is not a universal constant, as is often intimated, but is a function of body geometry and Reynolds number. Roshko (ref. 22) defines a "universal Strouhal number," S_R, which is not a function of body geometry, and is defined as

$$S_R = \frac{fh}{U_b} \tag{5}$$

where S_R = Roshko's "universal Strouhal number," with numerical value of about 0.17,

U_b = velocity just outside the boundary layer at the separation point, and

h = distance between rows of vortices after they become parallel.

The "universal Strouhal number" as defined by Roshko is, therefore, dependent on Reynolds number only to the extent that the existence of vortex street shedding is limited to certain Reynolds number ranges. Roshko (ref. 22) and Bearman (ref. 23) show that Roshko's "universal Strouhal number" is not valid for flows which involve wake interference elements such as splitter plates and base bleed; but these elements are not usually present in airfoil applications. With the use of Roshko's "universal Strouhal number," the vortex frequency may be determined provided U_b and h are known. For thin, streamlined bodies $U_b \approx U$ even when separation occurs near the maximum thickness. Data in reference 24 indicates that $U_b \approx 1.14U$ where separation occurred near the maximum thickness of an NACA 65(216)-222 airfoil at angles of attack of 8.1° and 10.1°. Thus, in this case, use of U rather than U_b in the Strouhal number definition affects the frequency by less than 15%. If we write

$$f = \frac{S_R U}{h}$$

then f is the frequency of the oscillatory lift force associated with the vortex street.

The wake thickness, h, is usually defined as being proportional to d, the projected dimension of the body perpendicular to the local resultant velocity. For thin airfoils at small angles of attack, d/c_i is given approximately by

$$d/c_i = (t_{max}/c_i) \cos \alpha + \sin \alpha$$

where t_{max} is the maximum thickness of the airfoil. No experimental results are known to be available which could be used to compare the h predicted by the form

$$h = (\text{constant}) \times (d)$$

with the h "when the rows of vortices become parallel," for use in Roshko's "universal Strouhal number" definition. An h/d = 1 has been used in reference 8, and an h/d = 1.54 was suggested in reference 25.

In order to determine vortex street noise there are a number of characteristics which must be defined. These characteristics include the frequency of the oscillatory drag associated with the vortex street, as compared to the frequency of the oscillatory lift; and the magnitude of the oscillatory vortex street lift and drag forces. The oscillatory drag force associated with the vortex street has twice the frequency of the oscillatory lift force when the body is symmetrical with respect to the free stream, as is the case for a circular cylinder or a symmetrical airfoil at zero lift. That is, the effect of the vortex arrangement at an instant in time on the pressure distribution about the body gives the same drag effect as a vortex arrangement one half cycle later. In figure 4, the two vortex street arrangements which are 180° out of phase are indicated by solid and dashed lines, respectively. When the body is not symmetrical with respect to the free stream, vortices one-half cycle apart do not necessarily give the same drag effect. Therefore, as angle of attack increases there is an increasingly important component of the oscillatory drag which has the same frequency as the oscillatory vortex lift. In addition, it is expected that the airfoils will operate most of the time at non-zero angles of attack. Therefore, only the component of oscillatory drag which has the same frequency as the oscillatory lift is considered in the present analysis.

An estimate of the magnitudes of the oscillatory vortex street lift and drag forces may be obtained on the basis of theoretical and experimental data. A dimensional analysis such as Yudin's (ref. 13) leads to an expression for the oscillatory lift and drag forces in terms of important flow parameters, body dimensions, and an unknown multiplying constant. The expression for the magnitude of the oscillatory lift force in terms of the circulation strengths of the vortices in the vortex street is

$$L_v = \text{constant } \rho(\Gamma/\ell)^2 h_0 \qquad (6)$$

where L_v = magnitude of the lift force per unit length,

Γ = circulation strength of an individual vortex in the vortex street,

ℓ = length between vortices in a row of the vortex street,

h_0 = a characteristic dimension of the body, and

ρ = density.

The theoretical form drag of a vortex street may be expressed as

$$D = \frac{\rho\Gamma^2}{2\pi\ell} + \frac{\rho\Gamma(U - 2u)h}{\ell} \quad . \tag{7}$$

This may be equated to the form drag expressed in terms of a coefficient of form drag for the vortex street, CD_v, as

$$D = CD_v(1/2\rho U^2 c) . \tag{8}$$

The circulation may be removed from the lift force expression by solving for Γ from the vortex street drag expressions, eqs. (7) and (8), or by using von Karman's stability condition that $h/\ell = 0.2806$, for which $\Gamma = \sqrt{8}\ell u$. The oscillatory lift force magnitude may then be expressed in the form

$$L_v = \text{constant } \rho\left(\frac{cVCD_v}{h}\right)^2 h_0 \quad .$$

Yudin assumed that the total drag is due to the vortex street, and that h_0 is equal to the projected body dimension, d. Eq. (7), combined with von Karman's stability criterion gives a theoretical expression for the vortex street drag in the form

$$D = \rho h U^2 \left[2.83\left(\frac{u}{U}\right) - 1.12\left(\frac{u}{U}\right)^2\right]$$

where D = steady drag force per unit span.

It is assumed that the vortex street form drag is equal to the steady incompressible drag. For this assumption, by equating Yudin's expression for the drag to that of eq. (8), the following relationship can be obtained:

$$1.12\left(\frac{u}{U}\right)^2 - 2.83\left(\frac{u}{U}\right) + \frac{CD_v}{2}\left(\frac{c}{h}\right) = 0 \quad .$$

Now it is assumed that both (u/U) and $CD_v/2\,(c/h)$ are small, so solving the above equation for u/U gives an approximate expression of

$$\frac{u}{U} \simeq 0.176\ CD_v\left(\frac{c}{h}\right) \quad .$$

From the expression for the magnitude of the oscillatory vortex street lift force as given in eq. (6) and using $h_0 = h$ and $\Gamma = \sqrt{8}\ell u$, L_v may be written

$$L_v = \text{constant}\ \rho(8u^2)h \quad .$$

For the (u/U) as given above in terms of CD_v and (h/c), the lift force magnitude becomes

$$L_v = \text{constant}\ \rho U^2\left[CD_v\left(\frac{c}{h}\right)\right]^2 h. \tag{9}$$

In terms of a constant of proportionality, k_L, and a lift coefficient for the vortex street, C_{LV},

$$L_v = C_{LV}(1/2\rho U^2 c)$$

where

$$C_{LV} = 2k_L(CD_v)^2\left(\frac{c}{h}\right).$$

Similarly, the drag force magnitude may be defined as

$$D_v = C_{DV}(1/2\rho U^2 c)$$

where $C_{DV} = 2k_D(CD_v)^2\left(\frac{c}{h}\right)$, and where k_D is a constant of proportionality. The functional dependence of k_L and k_d on CD_v and h/c, and an estimate of the magnitude of k_L may be obtained from theoretical expressions due to Lamb (ref. 26) and Blokhintsev (ref. 21). It is found that for circular cylinders with vortex shedding that

$$k_L = K_L(h/c)/CD_v \quad .$$

It can be determined that $K_L \simeq 0.09$, as an estimate of magnitude. For this form for k_L, and assuming the same form for k_D, the vortex street lift and drag force magnitudes for airfoils are assumed to be

$$L = K_L \rho U^2 c \Delta r CD_v \tag{10}$$

and

$$D = K_D \rho U^2 c \Delta r CD_v \tag{11}$$

where K_L and K_D are vortex street constants for lift and drag and are to be determined.

Lighthill (ref. 29) points out that sound intensity is not always proportional to $(\Delta r)^2$ as was assumed by Lamb and Blokhintsev, but that it is proportional to $(\Delta r)(\ell_c)$, where ℓ_c varies with Reynolds number, and is called a correlation length. This length is that within which lift fluctuations are well correlated. The correlation length generally decreases with increasing Reynolds number from Δr to the order of magnitude of the projected body dimension, d. The effect of using $(\Delta r)(\ell_c)$ instead of Δr^2 on eqs. (10) and (11) is that Δr would be replaced by $(\Delta r\, \ell_c)^{1/2}$. It was assumed that $\ell_c = \Delta r$ for all the results reported herein. Cancellation of noise between various radial and azimuthal stations is allowed.

It is noted, however, that the work of Etkin, et al., (ref. 27) indicates that $K_L = 0.09$ as determined by the preceding theoretical approach for circular cylinders is approximately one-fifth the magnitude of that found by experimental methods. They also indicate that based on experimental results the order of magnitude of the oscillatory drag force is about one-tenth the oscillatory lift force magnitude, and occurred at twice the lift force frequency. Work reported by Foughner and Duncan (ref. 28) indicated that for large circular cylindrical bodies the magnitude of the oscillatory drag was about one half of the oscillatory list force magnitude. Based on the above noted experimental work, $K_L \simeq 0.1$ to 1.0 and $K_D \simeq 0.05$ to 0.5 might be expected.

No measurements of the magnitude of the vortex street lift and drag forces are known to exist for airfoils. The method by which estimated values of K_L, K_D for airfoils were determined for use in

predicting the vortex street and rotational noise characteristics of helicopters is outlined below.

It was assumed that the difference between the experimentally measured and the theoretically predicted noise levels for arbitrary assumed values of K_L and K_D is due to incorrect magnitude of the assumed vortex street constants. While the experimentally measured sound pressure is a continuous spectrum, it was assumed that the proper values for the vortex street constants are those values which make the theoretical noise levels approximate the level of the off-harmonic noise levels above the fourth harmonic. Since there are more points for which agreement should exist than there are constants, the constants are determined by a least squares fit approach.

The possibility that K_L and K_D, as determined by the least squares fit method are underestimated exists because the sum of the separate rms pressures is greater than or equal to the rms pressure of the sum. That is, it cannot be assumed that the lift and drag pressures are always reinforcing. It is also apparent that the vortex street noise and the rotational noise are not necessarily reinforcing. In order to minimize the cancellation effects of these two sources, the vortex street noise constants were determined on the basis of a least squares fit on the $4^{\underline{th}}$ through $20^{\underline{th}}$ harmonics for the HU-1A helicopter in hover. The magnitude of the rotational noise is small in most of these harmonics, so that cancellation effects between the vortex and rotational noise should be negligible. The use of the turbine powered HU-1A helicopter also minimized the cancellation effects of engine noise in the determination of the vortex street constants. Tail rotor is still present, of course, as are other noise sources such as turbulent stresses, thickness effects, and gear boxes. It is interesting to note that when the vortex street constants were determined for the H-34 helicopter, for which large amounts of engine noise were present in the frequency spectrum of interest, approximately the same values for the constants were obtained.

As a result of this method as outlined, the vortex street lift and drag force magnitudes and frequencies are determined at each point in the rotor disc. Most of the required quantities, such as resultant velocity, angle of attack, and incompressible drag coefficients were already present in the computer program as they were used in computing rotational noise. Now the means of estimating the vortex street force magnitude and frequency have been established, and the oscillatory lift and drag may be expressed as functions of time and rotor disc location as

$$L_{v_{ij}}(t) = C_{LV_{ij}} \left| 1/2\rho \left(U_{ij} \right)^2 \right| c_i \, \Delta r_i \qquad (12)$$

where

$$C_{LV_{ij}} = 2 K_L CD_{V_{ij}} \sin \left(\omega_{ij} t + \phi_{ij} \right)$$

and

$$D_{V_{ij}}(t) = C_{DV_{ij}} \left[1/2 \rho \left(U_{ij} \right)^2 \right] c_i \Delta r_i \qquad (13)$$

where

$$C_{DV_{ij}} = 2 K_D CD_{V_{ij}} \sin \left(\omega_{ij} t + \phi_{ij} \right) .$$

The ϕ_{ij} is the phase of the vortex street lift at the beginning of the $j^{\underline{th}}$ azimuthal segment at the $i^{\underline{th}}$ radial station, and ω_{ij} is determined by the relationship

$$\omega_{ij} = \frac{2\pi S \, U_{ij}}{h_{ij}} .$$

Representation of Forces and Determination of Pressures

The forces on the fluid are those which cause the rotor to experience, as reactions, lift and drag. An area element of the swept surface may be thought of as having such forces on it as arise from calculating a force per unit of projected blade area and then multiplying by the differential of swept area. Regardless of whether these forces arise because of viscous effects or dynamic pressure effects they are replaced by an equivalent dipole source. Radiation from a dipole has directionality and the orientation of the force vector at a source point determines the orientation of the dipole source, and thus its directional sound pressure radiation pattern.

As each rotor blade passes through an element of the swept surface, pressure pulses are created and may be expressed as a force per unit area. The duration of these pulses is τ_{ij}, and it is assumed that they recur after a period, T, as shown in figure 5.

The assumption that the rotational noise is periodic is a reasonable assumption; however, the vortex street noise is not necessarily periodic. The method that is being extended (ref. 9) to include vortex noise assumes periodicity, so to include vortex noise effects with this analysis technique the vortex forces must also be periodic, regardless of their frequency. In order that the vortex street noise be periodic, its magnitude, frequency, and phase must be periodic. The magnitude and frequency of the vortex street noise are assumed to be functions of free stream speed, density, and incompressible drag coefficient, which are constant at a particular radial and azimuthal point. Therefore, the magnitude and frequency of the vortex street is the same for every blade at a given radial and azimuthal station, so these quantities are periodic with the blade passage frequency. The phase of the vortex street is not necessarily periodic in the real physical situation. That is in general,

$$\int_0^{2\pi} \frac{\omega}{\Omega} \, d\psi \neq (2\pi) \times (\text{integer}).$$

In the numerical integration technique used herein the vortex street phase may be discontinuous at various points in the rotor plane. Discontinuities may occur at the "starting point," say $\psi = 0$, of the rotor blade since $\sum_{j=1}^{N} (\omega_j \, \Delta\psi_j/\Omega)$ is not necessarily equal to 2π times an integer, and for such a case the phase is assumed to be discontinuous at $\psi = 0$.

This assumption is necessary in order that the vortex street be periodic. Other discontinuities in phase occur as a result of assumed constant physical flow properties over each azimuthal section. The amplitude at the intersection of neighboring azimuthal stations is made continuous if possible, and where maximum amplitude and frequency are different in these neighboring sections the phase will generally have a small discontinuity. It is possible that the amplitude of the $j^{\underline{th}}$ section may be greater than that of the $j + 1^{\underline{st}}$ section, and the phase may be near $\pm 90°$. The maximum amplitude of the $j + 1^{\underline{st}}$ section may be smaller than that of the $j^{\underline{th}}$ section, which does not permit a continuous amplitude. In this case, the amplitude of the $j + 1^{\underline{st}}$ section is assumed to be at

its peak value at the interface, which minimizes the discontinuity in amplitude and results in a small discontinuity in phase.

If the blade chord length is c_i and the blade geometric angle is θ_{ij}, then the projection of the chord length on the swept surface is $c_i \cos \theta_{ij}$ and $\tau_{ij} = \frac{c_i \cos \theta_{ij}}{r_i \Omega}$. To avoid the complications which otherwise arise, it will be assumed that

$$c_i \cos \theta_{ij} \simeq c_i \cos \theta_i \equiv c_i' \text{ and } \tau_{ij} \simeq \tau_i \equiv \frac{c_i'}{r_i \Omega} ,$$

where θ_i is the mean pitch angle at a given radius. Since

$$\theta_{ij} = \theta_0 + \theta_1 \cos \psi_j + \theta_2 \sin \psi_j - \frac{q(r_i - e)}{R - e}$$

where q is the twist built into the blade, approximating θ_{ij} by θ_i is tantamount to neglecting the cyclic pitch angles θ_1 and θ_2. This approximation is only made in the calculation of τ_i.

The shape of the pulses over the time τ_i, depends on the distribution of force over the chord. It can be assumed with little error that only the magnitude of the pressure pulses as shown in figures 6(a), (b), and (c) which are assumed to represent the steady lift, incompressible drag, and wave drag, respectively, vary with azimuth, and that their shapes are constant. Similarly, the magnitude of the oscillatory vortex street forces vary with azimuth, as do the frequency and phase, but the shapes as shown in figure 6(d) are assumed to be similar around the azimuth. In reference 5, the effect of chordwise force distribution is discussed at some length as having an appreciable effect on the higher harmonics of rotor noise. Since rotor "bang" or "slap" noise as reported in references 7 and 30 is a relatively high frequency phenomenon and is such an important aspect of rotor noise, the chordwise distribution differences have been purposely retained in this report in the analysis of this phenomena as was done in reference 9 for the rotational noise only. The oscillatory vortex street forces are high frequency sources, and are assumed to act uniformly over the chord. For a constant magnitude of the pressure pulses due to the steady lift and drag forces, their shapes can be expressed as a real Fourier series:

$$f_i = a_{0_i} + \sum_{m=1}^{\infty} (a_{m_i} \cos mB\Omega t + b_{m_i} \sin mB\Omega t).$$

Note that the shape function, f_i, can be thought of as a function either of the coordinate which measures the chord length projection on the swept surface, c_i, or of the time, t. This function is thought of as beginning at t = 0, which coincides with $\psi = 0$. For convenience, the coefficients a_{0_i}, a_{m_i} and b_{m_i} are normalized so that $f_{i_{max}} = 1.0$. To account for the variation in the magnitude of the lift and drag around the azimuth, normalization factors for these Fourier coefficients must be established. Since the shape represented by the normalized coefficients has been specified to have a maximum ordinate equal to unity, the aerodynamic lift acting on a span length Δr_i is

$$L_{ij}(t) = C_{L_{ij}} \; 1/2 \; \rho (U_{ij})^2 c_i \; \Delta r_i \equiv \bar{\kappa}_{ij} \int_{\text{chord}} \bar{f}_i \; dc_i' \; \Delta r_i$$

where $\bar{\kappa}_{ij}$ = normalization factor for lift,

U_{ij} = resultant relative wind velocity normal to blade leading edge,

ρ = air mass density, and

$C_{L_{ij}}$ = lift coefficient.

Similarly, for incompressible profile drag

$$D_{C_{ij}}(t) = C_{D_{ij}} \; 1/2 \; \rho (U_{ij})^2 c_i \; \Delta r_i \equiv \bar{\bar{\kappa}}_{ij} \int_{\text{chord}} \bar{\bar{f}}_i \; dc_i' \; \Delta r_i,$$

and for compressible (wave) drag

$$D_{w_{ij}}(t) = C_{D_{w_{ij}}} 1/2\rho(U_{ij})^2 c_i \Delta r_i \equiv \bar{\bar{\kappa}}_{ij} \int_{\text{chord}} \bar{\bar{f}}_i \, dc_i' \, \Delta r_i \quad .$$

Since sound is an oscillatory phenomenon, the steady term in the Fourier series may be dropped. The Fourier series may therefore be written in the form

$$\bar{\bar{f}}_i = \sum_{m=1}^{\infty} (c_{m_i} \cos mB\Omega t + \Psi L_{m_i} \sin mB\Omega t) \quad .$$

Since two lift forces (due to steady and vortex street lift) are combined, as well as the three drag forces (due to steady incompressible and compressible and vortex street drag), it is convenient to leave the forces in the above form until the required additions are performed. Therefore, the normalized coefficients c_{m_i} and ΨL_{m_i} are associated with the blade lift, by the equation directly above, then two more sets of similar relationships associated with (1) incompressible drag, in which d_{m_i} and Γ_{m_i} are the Fourier coefficients, and (2) compressibility drag, in which e_{m_i} and KD_{m_i}, are the Fourier coefficients, may also be established.

Analytical expressions for such Fourier constants are derived by the usual means (see, for example, ref. 31), for the three chordwise shapes shown in figures 6(a) through 6(c). The selection of these shapes as approximations for lift, incompressible drag and wave drag was based on a perusal of two-dimensional section data below stall, and computational convenience.

The corresponding formulae are as follows:

$$C_{m_i} = \frac{1}{Tm\pi} [d(1 - \cos T) + \frac{\ell}{a}(1 - \cos aT)]$$

$$\Psi L_{m_i} = \frac{1}{Tm\pi} [T - (d \sin T + \frac{\ell}{a} \sin aT)]$$

$$d_{m_i} = \frac{\sin T}{m\pi}$$

$$\Gamma_{m_i} = \frac{1}{m\pi} (1 - \cos T)$$

$$e_{m_i} = \frac{r_i}{c_i' Bm^2\pi(1-f)(f-g)} [(1 - g) \cos fT - (1 - f) \cos gT - (f - g) \cos T]$$

$$KD_{m_i} = \frac{r_i}{c_i' Bm^2\pi(1-f)(f-g)} [(1 - g) \sin fT - (1 - f) \sin gT - (f - g) \sin T] \qquad (14)$$

where $T = \frac{mBc_i'}{r_i}$

(These equations differ from equations (3) of reference 9 for two reasons. Equations (3) of reference 9 are in polar form, for the respective forces, and equations (14) are not. Also, the magnitude terms of equations (3) of reference 9 were incorrect in that the left-hand sides should not have been divided by the force integral term). In a similar manner, the oscillatory lift due to the vortex street acting on a span of length Δr_i is

$$L_{V_{ij}}(t) = C_{LV_{ij}} 1/2\rho (U_{ij})^2 c_i \Delta r_i$$

and the oscillatory drag due to the vortex street is

$$D_{V_{ij}}(t) = C_{DV_{ij}} 1/2\rho (U_{ij})^2 c_i \Delta r_i ,$$

where $C_{LV_{ij}}$ and $C_{DV_{ij}}$ are vortex street lift and drag coefficients and are functions of time. For vortex lift and drag of peak magnitude 1.0,

$$\sin(\omega_{ij} t + \phi_{ij}) = \sum_{m=1}^{\infty} (CV_{m_{ij}} \cos mB\Omega t + \Psi V_{m_{ij}} \sin mB\Omega t)$$

Therefore, the coefficients $CV_{m_{ij}}$ and $^{\psi}V_{m_{ij}}$ are associated with the vortex street lift, by the equation directly above. One more set of quantities associated with vortex street drag, say $dV_{m_{ij}}$ and $KV_{m_{ij}}$ may be defined by this same equation, since the lift and drag have been assumed to have the same phase and frequency. The selection of the shape as shown in figures 6(d) as approximations for the oscillatory vortex street lift and drag is based on the assumption that the vortex lift and drag are uniform over the chord and oscillate with frequency ω, determined from the Strouhal number definition. The corresponding formulae are as follows:

$$CV_m = \frac{B\Omega}{2\pi}\left[\cos\phi\left(\frac{1-\cos(\omega-mB\Omega)\tau}{\omega-mB\Omega}+\frac{1-\cos(\omega+mB\Omega)\tau}{\omega+mB\Omega}\right)\right.$$
$$\left.+\sin\phi\left(\frac{\sin(\omega-mB\Omega)\tau}{\omega-mB\Omega}+\frac{\sin(\omega+mB\Omega)\tau}{\omega+mB\Omega}\right)\right]$$

$$^{\psi}V_m = \frac{B\Omega}{2\pi}\left[\cos\phi\left(\frac{\sin(\omega-mB\Omega)\tau}{\omega-mB\Omega}-\frac{\sin(\omega+mB\Omega)\tau}{\omega+mB\Omega}\right)\right.$$
$$\left.+\sin\phi\left(\frac{1-\cos(\omega+mB\Omega)\tau}{\omega+mB}-\frac{1-\cos(\omega-mB\Omega)\tau}{\omega-mB\Omega}\right)\right] \qquad (15)$$

where τ is understood to be subscripted by i, and CV_m, $^{\psi}V_m$, ϕ, and ω are understood to be subscripted by ij. For the special case where $\omega = mB\Omega$

$$CV_m = \frac{1}{2\pi m}\left[\cos\phi\,\sin^2\omega\tau+\sin\phi\left(\tau mB\Omega+\frac{\sin 2\omega\tau}{2}\right)\right]$$

$$\psi V_m = \frac{1}{2\pi m}\left[\sin\phi\,\sin^2\omega\tau+\cos\phi\left(\tau mB\Omega+\frac{\sin 2\omega\tau}{2}\right)\right]$$

The coefficients for the vortex street drag, $dV_{m_{ij}}$ and $KV_{m_{ij}}$ are

equal to $CV_{m_{ij}}$ and $\Psi V_{m_{ij}}$, respectively, since the vortex street lift and drag forces have the same phase and frequency. The difference in magnitude between the vortex street lift and drag forces is due to the difference in magnitude of the vortex street lift constant $CSVL_{ij}$, and the vortex street drag constant CVD_{ij}.

Note that the lift, incompressible drag, wave drag, and the vortex street lift and drag coefficients are all functions of (1) local relative velocity Mach number, $M_{N_{ij}}$, and (2) local aerodynamic angle of attack, α_{ij}.

It is convenient to express the combination of the rotational and vortex street forces in polar form. Let

$$a_m = \left[\left(C_L \frac{C_m}{\int_{\text{chord}} \bar{f}\, dc'} + CSVL \cdot CV_m \right)^2 + \left(C_L \frac{\Psi L_m}{\int_{\text{chord}} \bar{f}\, dc'} + CSVL \cdot \Psi V_m \right)^2 \right]^{1/2}$$

$$\Psi_m = \arctan \left(\frac{C_L \dfrac{C_m}{\int_{\text{chord}} \bar{f}\, dc'} + CSVL \cdot CV_m}{C_L \dfrac{\Psi L_m}{\int_{\text{chord}} \bar{f}\, dc'} + CSVL \cdot \Psi V_m} \right)$$

$$b_m = \left[\left\{C_{D_C} \frac{d_m}{\int_{\text{chord}} \bar{\bar{f}}\, dc'} + C_{D_W} \frac{e_m}{\int_{\text{chord}} \bar{\bar{f}}\, dc'} + C_{VD} \cdot dV_m\right\}^2 + \left\{C_{D_C} \frac{\Gamma_m}{\int_{\text{chord}} \bar{\bar{f}}\, dc'} + C_{D_W} \frac{KD_m}{\int_{\text{chord}} \bar{\bar{f}}\, dc'} + CVD \cdot KV_m\right\}^2\right]^{1/2}$$

$$\kappa_m = \arctan \left(\frac{C_{D_C} \frac{d_m}{\int_{\text{chord}} \bar{\bar{f}}\, dc'} + C_{D_W} \frac{e_m}{\int_{\text{chord}} \bar{\bar{f}}\, dc'} + CVD \cdot dV_m}{\frac{\Gamma_m}{\int_{\text{chord}} \bar{\bar{f}}\, dc'} + C_{D_W} \frac{KD_m}{\int_{\text{chord}} \bar{\bar{f}}\, dc'} + CVD \cdot KV_m} \right) \qquad (16)$$

where c_m, ΨL_m, d_m, Γ_m, e_m, KD_m, $\bar{\bar{f}}$, $\bar{\bar{f}}$, $\bar{\bar{f}}$, and dc' are understood to be subscripted by i, and a_m, Ψ_m, C_L, $CSVL$, CV_m, ΨV_m, C_{D_C}, C_{D_W}, CVD, dV_m, and KV_m, b_m, κ_m are understood to be subscripted by ij.

The m^{th} component of lift associated with a given pressure pulse (assumed to start at time $t = 0$), may now be expressed in the form

$$\text{Re}\left[L_{m_{ij}} e^{imB\Omega t}\right] = \text{Re}\left[1/2\rho(U_{ij})^2 c_i r_i \Delta r_i a_{m_{ij}} e^{i\left(mB\Omega t - \Psi_{m_{ij}}\right)}\right] .$$

To allow for the fact that these pulses do not always start at $t = 0$, but at time $t + \psi_j/\Omega$, multiply the right-hand side of the above equation by the factor

$$e^{-imB\Omega(\psi_j/\Omega)} = e^{-imB\psi_j}$$

where

ψ_j = increment in azimuth angle from one station on the swept area to another,

j = 1, 2, 3...n

n = total number of azimuthal sections into which the swept area is divided,

m = harmonic number, and

B = number of blades.

From these definitions it follows that the $m^{\underline{th}}$ harmonic component of the forces experienced by the fluid due to blade lift and drag may be expressed as the following:

$$\mathrm{Re}\left[L_{m_{ij}} e^{imB\Omega t}\right] = -\mathrm{Re}\left[1/2\rho(U_{ij})^2 c_i r_i \Delta r_i \Delta\psi_i a_{m_{ij}} e^{i(mB\Omega t - \Psi_{m_{ij}} - mB\psi_j)}\right]$$

and

$$\mathrm{Re}\left[D_{m_{ij}} e^{imB\Omega t}\right] = -\mathrm{Re}\left[1/2\rho(U_{ij})^2 c_i r_i \Delta r_i \Delta\psi_i b_{m_{ij}} e^{i(mB\Omega t - \kappa_{m_{ij}} - mB\psi_j)}\right] \quad (17)$$

In order that these sinusoidally varying forces be evaluated or expressed in terms of components along the Cartesian coordinate axes, it is necessary to account for the direction and magnitude of the resultant velocities U_{ij} (since lift and drag forces are defined as perpendicular and parallel to them, respectively). Equations (4) give the required transformation. With the Fourier coefficients of the Cartesian coordinate components of the blade

forces known, the harmonics of the pressure at a given field point may be computed from equation (2). Now to use equation (2) to calculate $m^{\underline{th}}$ harmonic of sound pressure at a field point (x_0, y_0, z_0) due to the $m^{\underline{th}}$ harmonic oscillatory pressure at a source point identified by the indices i, j, note that

$$\frac{\partial}{\partial x_0}\left(\frac{e^{-ik_m\sigma_{ij}}}{S_{ij}}\right) = -\frac{e^{-ik_m\sigma_{ij}}}{S_{ij}}\left[\frac{ik_mM_N}{\gamma^2} + \left(\frac{ik_m}{\gamma^2} + \frac{1}{S_{ij}}\right)\left(\frac{x_0-x}{S_{ij}}\right)\right]$$

$$\frac{\partial}{\partial y_0}\left(\frac{e^{-ik_m\sigma_{ij}}}{S_{ij}}\right) = -\frac{e^{-ik_m\sigma_{ij}}}{(S_{ij})^2}\left(ik_m + \frac{\gamma^2}{S_{ij}}\right)(y_0-y)$$

$$\frac{\partial}{\partial z_0}\left(\frac{e^{-ik_m\sigma_{ij}}}{S_{ij}}\right) = -\frac{e^{-ik_m\sigma_{ij}}}{(S_{ij})^2}\left(ik_m + \frac{\gamma^2}{S_{ij}}\right)(z_0-z) \qquad (18)$$

Then substitution of $L_{m_{ij}}$ and $D_{m_{ij}}$ from equation (17) for lift and drag, respectively, in equation (4), and substitution of the resulting force components and the relationships defined in equation (18) into equation (2) yields the desired expressions for the pressure at the field point. The resulting equations can be broken into real and imaginary parts and, after algebraic manipulation, cast in the following form:

$$P_m(x_0,y_0,z_0)_{ij_R} = \frac{1}{4\pi}\frac{K_{ij}}{(S_{ij})^2}\left\{\bar{A}_{ij}\left[\bar{K}_{m_{ij}}\sin\phi_{ij} - \bar{L}_{m_{ij}}\cos\phi_{ij}\right]\right.$$

$$- \bar{B}_{ij}\left[\bar{K}_{m_{ij}}\cos\phi_{ij} + \bar{L}_{m_{ij}}\sin\phi_{ij}\right]$$

$$+ \frac{S_{ij}M_Nk_m}{\gamma^2}\left[\bar{G}_{m_{ij}}\left(\bar{I}_{ij}\cos\phi_{ij} - \bar{J}_{ij}\sin\phi_{ij}\right)\right.$$

$$\left.\left. - \bar{E}_{m_{ij}}\left(\bar{I}_{ij}\sin\phi_{ij} + \bar{J}_{ij}\cos\phi_{ij}\right)\right]\right\}$$

$$P_m(x_0,y_0,z_0)_{ij_I} = \frac{1}{4\pi}\frac{K_{ij}}{(S_{ij})^2}\left\{\bar{A}_{ij}\left[\bar{D}_{m_{ij}}\sin\phi_{ij} + \bar{C}_{m_{ij}}\cos\phi_{ij}\right]\right.$$

$$- \bar{B}_{ij}\left[\bar{D}_{m_{ij}}\cos\phi_{ij} - \bar{C}_{m_{ij}}\sin\phi_{ij}\right]$$

$$+ \frac{S_{ij}M_N k_m}{\gamma^2}\left[\bar{H}_{m_{ij}}(\bar{I}_{ij}\cos\phi_{ij} - \bar{J}_{ij}\sin\phi_{ij})\right.$$

$$\left.\left. - \bar{F}_{m_{ij}}(\bar{I}_{ij}\sin\phi_{ij} + \bar{J}_{ij}\cos\phi_{ij})\right]\right\} \quad (19)$$

where

$$\bar{A}_{ij} = \gamma^2(y_0 - y_{ij})\cos\psi_j$$

$$- \left[(x_0 - x_{ij})\cos\alpha_s + \gamma^2(z_0 - z_{ij})\sin\alpha_s\right]\sin\psi_j$$

$$\bar{B}_{ij} = (x_0 - x_{ij})\bar{J}_{ij} + \gamma^2\left[(y_0 - y_{ij})\beta_j\sin\psi_j\right.$$

$$\left. + (z_0 - z_{ij})(\beta_j\cos\psi_j\sin\alpha_s + \cos\alpha_s)\right]$$

$$\bar{C}_{m_{ij}} = \frac{\bar{G}_{m_{ij}}}{S_{ij}} - \frac{k_m\bar{H}_{m_{ij}}}{\gamma^2}$$

$$\bar{D}_{m_{ij}} = -\frac{\bar{E}_{m_{ij}}}{S_{ij}} + \frac{k_m\bar{F}_{m_{ij}}}{\gamma^2}$$

$$\bar{E}_{m_{ij}} = a_{m_{ij}}\sin(k_m\sigma_{ij} + \Psi_{m_{ij}} + mB\psi_j)$$

$$\bar{F}_{m_{ij}} = a_{m_{ij}} \cos (k_m \sigma_{ij} + \Psi_{m_{ij}} + mB\psi_j)$$

$$\bar{G}_{m_{ij}} = b_{m_{ij}} \sin (k_m \sigma_{ij} + \kappa_{m_{ij}} + mB\psi_j)$$

$$\bar{H}_{m_{ij}} = b_{m_{ij}} \cos (k_m \sigma_{ij} + \kappa_{m_{ij}} + mB\psi_j)$$

$$\bar{I}_{ij} = \cos \alpha_s \sin \psi_j$$

$$\bar{J}_{ij} = \beta_{ij} \cos \alpha_s \cos \psi_j - \sin \alpha_s$$

$$\bar{K}_{m_{ij}} = \frac{\bar{F}_{m_{ij}}}{S_{ij}} + \frac{k_m \bar{E}_{m_{ij}}}{\gamma^2}$$

$$\bar{L}_{m_{ij}} = \frac{\bar{H}_{m_{ij}}}{S_{ij}} + \frac{k_m \bar{G}_{m_{ij}}}{\gamma^2}$$

$$K_{ij} = 1/2 \rho c_i (U_{ij})^2 r_i \Delta\psi \Delta r_i$$

$$S_{ij} = \{(x_0 - x_{ij})^2 + \gamma^2[(y_0 - y_{ij})^2 + (z_0 - z_{ij})^2]\}^{1/2}$$

$$\sigma_{ij} = \frac{M_N(x_0 - x_{ij}) + S_{ij}}{\gamma^2}$$

and $a_{m_{ij}}$, and $b_{m_{ij}}$, $\Psi_{m_{ij}}$, and $\kappa_{m_{ij}}$ are defined in equations (16).

The integration proceeds by independently summing all the real and imaginary parts of the oscillatory pressure of harmonic m, contributed to by all the combinations of i and j. If P_{m_R} and P_{m_I} are in psi, then the sound pressure level, SPL, in decibels (referred to 0.0002 dynes/cm) is

$$SPL = 10 \log_{10}\left\{\frac{1}{2}\left|\frac{478.8}{0.0002}\right|^2\left[\left(\sum_i \sum_j P_{m_{ij_R}}\right)^2 + \left(\sum_i \sum_j P_{m_{ij_I}}\right)^2\right]\right\} . \qquad (20)$$

The pressure as a function of time at a particular field point may be expressed in the form

$$P(t) = a_0/2 + \sum_{m=1}^{\infty} (a_m \cos mB\Omega t + b_m \sin mB\Omega t).$$

In practice, a limited number of harmonics are used, and a_0 is unimportant since it contributes no time variation to P(t). Thus, the pressure as a function of time can be computed from the expression

$$P(t) = \sum_{m=1}^{KHI} (a_m \cos mB\Omega t + b_m \sin mB\Omega t) \qquad (21)$$

where KHI is the maximum number of harmonics used, and where

$$a_m = \sum_i \sum_j P_{m_{ij_R}} ,$$

and

$$b_m = \sum_i \sum_j P_{m_{ij_I}} .$$

RESULTS AND DISCUSSION

This section of the report will first present and discuss results obtained to show the effects that a far field approximation has on the predicted noise characteristics of a thrusting rotor in axial flight. This will be followed by an evaluation of the pertinent characteristics of the experimental measurements with which the predicted noise will be compared. The manner in which the controlling shed vortex parameters were determined will then be presented. A comparison of measured and predicted SPL's for two different helicopters in hover flight will be made, and predicted SPL's for various flight conditions for one of the helicopters will be presented and discussed. Finally, predicted and measured pressure time histories will be presented.

Effects of Far Field Approximation

Part of the work reported in reference 9 was a comparison of the sound pressure level predicted with and without using a far field approximation. The results obtained using a far field approximation were based on a closed form solution developed by Garrick and Watkins (ref. 5). The results obtained without this approximation were based on the numerical integration technique presented in reference 9. This comparison was done for the first harmonic only. As an additional check on the effect of the far field approximation on the predicted noise, a similar check was made for a higher harmonic of the rotational noise. The results of this investigation are shown in figure 7. It is apparent from the form of the expression for the SPL and from the results shown in figure 7 that for all harmonics (1) the numerical integration duplicates the closed form solution where the closed form solution is correct, and (2) use of the far field approximation yields the sharp reduction in sound level predicted in the range of one to two diameters ahead of the propeller.

Agreement between the numerical integration results and the closed form solution results for values of X_0/D for which the closed form solution is valid is an indication of the accuracy of the integration method and computer program of the present analysis. Important features of the computer program which affect the numerical accuracy of the results are discussed in reference 9 and are incorporated in the present analysis.

Analysis of Experimental Measurements

Noise characteristics of helicopters are usually described on the basis of plots of sound pressure level versus frequency, or pressure time histories. Correct understanding and interpretation

of such experimental data is vital to the use of such data for comparison with theoretical data or to give proper direction to the development of analysis techniques.

The following discussion presents experimental data which will later be used for comparison with predicted results. It is necessary to understand the pertinent characteristics of the experimental data in order to make a meaningful comparison between theory and measurement. Data for the HU-1A and the H-34 are used in this report as a basis for such comparisons.

Table I presents the location of the field points in relation to the rotor hub in terms of cylindrical coordinates. These field points define the location of the observer in figure 8 and subsequent figures. Figure 8 shows the measured sound pressure level versus frequency curve for an HU-1A. Main rotor harmonic number locations are indicated. Instrumentation calibration characteristics, together with the SPL versus frequency plot give harmonic spacing within 2% of the spacing predicted for the normal rotor speed of 314 RPM. This error is well within that expected for rotor speed measurement. High amplitude off-harmonic peaks are not expected and do not occur for frequencies up to the fifth blade passage harmonic since the dominant source of noise in this frequency range is rotational noise from the main rotor which occurs only at the blade passage frequency. (The first main rotor harmonic is not recorded due to low frequency cut-off of the instrumentation).

Tail rotor noise is significant, as is seen from figure 8. Gear ratios and effectively inflexible shafting result in tail rotor harmonic spacing approximately 5.14 times the main rotor harmonic spacing.

The first five main rotor harmonic peaks and the first three or four tail rotor harmonic peaks are dominant in their respective frequency ranges, and come very near the expected frequencies. However, above the sixth main rotor harmonic (about 60 cps) there are off-harmonic peaks of the same order of magnitude as the main rotor peaks. Since the HU-1A has a turbine engine, the engine noise should be small at these relatively low frequencies. As may be seen from figure 8, the tail rotor harmonic spacing is uniform, which strongly suggests that the instrumentation is not causing frequency shifting of the peaks of the SPL versus frequency plot. However, peaks on the order of magnitude of main rotor noise peaks do occur at frequencies not identified as main rotor or tail rotor frequencies (and with spacing which is not main rotor harmonic spacing). Since the frequency scale appears to be reliable, and since peaks were measured at frequencies and with spacings which cannot be due to main or tail rotor peaks, these off-harmonic peaks must be due to another source which is not periodic with respect to main rotor or tail rotor blade passage. A nonuniform

rotor speed could result in blade loadings which differ from blade to blade at the same azimuth point, and thus produce off-harmonic noise. This however is not believed to be the case. Vortex shedding of the vortex street type is a noise source which is not periodic with respect to blade passage and which may account for some of the off-harmonic noise peaks that are observed.

Figure 9 shows a plot of SPL versus frequency for an H-34 helicopter with which theoretical predictions will be compared. The largest peaks that are observed do not generally occur near main rotor harmonic frequencies and have been identified as engine noise. The engine firing frequency is about 20.5 cps, and this is the spacing of SPL peaks marked by the letter E. The main rotor harmonic spacing is about 14.7 cps, and these harmonic positions have been indicated by M. (As with the HU-1A data, the first main rotor harmonic is not recorded due to low frequency cut-off of the instrumentation). Tail rotor harmonic positions are six times the main rotor harmonic spacing, and are marked T. It is noted that some of the larger peaks are due to a combination of engine-main rotor, or engine-tail rotor noise. It is noted that the peaks due to engine noise were not identified as such until after the publication of reference 9. Figure 9 data is for the exhaust side of the H-34, so the dominance of engine exhaust noise is not unexpected. Plots of SPL versus frequency for several other field points were studied however and engine noise still dominates although not always by the extent indicated in figure 9. As noted previously for the HU-1A, there are off-harmonic peaks for the H-34 of the same magnitude as the main rotor harmonic peaks above the 6^{th} main rotor harmonic. Both the HU-1A and the H-34 have approximately the same SPL values for main rotor harmonic positions, where the tail or engine noise effects are not dominant.

Comparison of the data presented in figures 8 and 9 show some important characteristics. First, the SPL of the main rotor harmonics do not drop off as rapidly as predicted by theories including only rotational noise. Rather, there is a very gradual decrease for the HU-1A and an increase followed by a decrease for the H-34. Second, the main rotor is not the dominant noise source over the entire frequency range. Engine noise is dominant for the H-34 and tail rotor noise is dominant for the HU-1A, for the particular field points of these measurements. Elimination of H-34 engine noise would leave main rotor,tail rotor and (especially above 100 cps) off-harmonic noise as the dominant noise sources. Elimination of HU-1A tail rotor noise leaves main rotor and off-harmonic noise as the dominant noise sources. Third, the off-harmonic peaks above approximately 100 cps are of the same order of magnitude as the main rotor noise peaks. Plots of SPL versus frequency for these two helicopters at other field points show essentially the same characteristics. The tail rotor noise for the HU-1A and the engine noise for the H-34 appear to be the dominant noise sources over most of the field. All published plots of SPL versus

frequency which are made with narrow bandwidth filters of 6 cps bandwidth or less show significant off-harmonic noise over portions of the frequency spectrum.

Theoretical Results and Comparison With Experiment

Vortex street type vortex shedding can contribute noise over a wide range of frequencies and may be the source of the observed off-harmonic peaks. The magnitude of the vortex street constants K_L and K_D of equations (10) and (11) respectively, are determined on the basis that the vortex street noise should be on the order of the off-harmonic noise level. The theoretical method assumes that identical events take place at the same azimuthal positions regardless of particular blade or its passage. It, therefore, computes noise only at main rotor harmonic frequencies. Although disordered vortex shedding may invalidate this assumption, nevertheless, the vortex street noise levels were assumed to occur at the main rotor harmonics and were used to evaluate the vortex street constants. The vortex shedding frequency is an important factor in the computation of the magnitude of the Fourier coefficients of the vortex street noise and is inversely proportional to the distance between the rows of vorticies shed from a particular blade at any time. While this distance is known for cylinders, no such measurements are known to exist for airfoils at low angles of attack, and, therefore, values of h/d of 1.0 and 1.54 as suggested in references 8 and 25 respectively, were used in computing the vortex street constants, K_L and K_D. The values of K_L and K_D as computed by the method of least squares fit varied for different field points and h/d ratio. Generally $0.5 \leq K_L \leq 1.0$ and $0.1 \leq K_D \leq 0.5$ resulted. Because of cancellation effects these values of K_L and K_D are order of magnitude estimates. While various K_L and K_D values were used to study the effect of these parameters, $K_L = 1.0$ and $K_D = 0.5$ seemed to give good correlation for several field points, so they were used for most of the computations. These values of K_L and K_D give vortex street lift and drag force magnitudes of the order of the steady drag force for an airfoil, and therefore seem reasonable. Experiments should be conducted to determine their numerical values more accurately.

Figure 10 shows a comparison between the measured SPL's and the computed SPL's at main rotor harmonics for an HU-1A helicopter for an h/d of 1.54 and for different values of K_L and K_D. (Note that SPL values are computed at main rotor harmonic frequencies only. The lines joining the data points are for ease of identification, and do not represent a continuous SPL versus frequency

spectrum). The rotational only ($K_L = 0$, $K_D = 0$) noise shown in figure 10 is the same as computed in reference 9. In general, for K_L, $K_D > 0$, there is a significant increase of predicted noise above the seventh harmonic. The larger values of K_L and K_D give larger SPL values, except where there is almost complete cancellation between the various sources, such as at the eighteenth harmonic, and to a limited degree for the twelfth harmonic. All of the predicted SPL values are very close to the rotational values for the low harmonics, so the SPL's for the nonrotational noise sources are shown only as they become distinct from the rotational noise SPL's on this and subsequent plots of SPL versus harmonic number. There is substantial improvement between the predicted and measured SPL with the inclusion of vortex street noise in addition to rotational noise. The largest peaks of the measured SPL values are near the tail rotor harmonics. There is no representation of the tail rotor in the predicted SPL, so no comparison should be made at these points. The predicted SPL values fall below the harmonic peaks at all harmonics. However, the predicted values do come closer to the level of the off-harmonic noise.

Figure 11 shows the measured and computed SPL values with two different h/d values for the vortex noise computation. The value of h/d of 1.54 gives generally better agreement with the measured SPL values than does the value of h/d of 1. Both the SPL values individually, and the trend with increasing harmonic number appear to be better for an h/d of 1.54. Except for the results for h/d of 1.0 for harmonic numbers 10 and 11, which are probably due to cancellation effects, comparison of the results presented in figures 10 and 11 indicate that the parameters K_L and K_D are more significant than h/d. Because of the results shown in figures 10 and 11, and because of additional results that have not been presented, the values of h/d of 1.54, K_L of 1.0, and K_D of 0.5 were used in computing SPL values and pressure time histories for the HU-1A and the H-34 in hover, and for the H-34 in various flight conditions.

As may be seen from figures 10 and 11, there is considerable improvement between predicted and measured SPL values with the inclusion of vortex street effects. However, there remains a rather serious lack of agreement at the harmonic peaks. As previously mentioned, only sources which are periodic should be expected to result in such peaks. There are several possible reasons why the present predicted rotational noise is below the measured noise, particularly in the higher harmonics. One is that possible noise sources, such as blade thickness effects, have been neglected in this analysis. The high peaks near the $5^{\underline{th}}$, $10^{\underline{th}}$, $15^{\underline{th}}$, and $20^{\underline{th}}$ harmonics for the HU-1A are most likely due to tail rotor noise, which has not been included. Perhaps

more important is the lack of sufficient data to accurately determine the high frequency content of the measured airloads. Airload measurements made and recorded with high frequency response instrumentation would provide a significantly improved foundation for noise prediction methods based on measured airloads (which are the basis of all current rotational noise prediction methods).

The vortex street constants as determined for the HU-1A in hover were used to compute the sound pressure levels for the H-34 in hover, and in forward and steep descent flight conditions. The results of these computations are shown plotted in figures 12 through 15.

As may be seen from figure 12, the inclusion of vortex noise has similar results for the H-34 as for the HU-1A in hover. There is significant improvement in the agreement between the measured and predicted noise with the use of the same values of h/d, K_L and K_D as were used for the HU-1A. Measured off-harmonic peaks exist above the sixth harmonic, and the predicted noise is of approximately the same level as this off-harmonic noise.

Figure 13 shows the plot of SPL versus harmonic number for a steep descent flight condition. Experimental airload data was taken from reference 16. This case was chosen because it was indicated in reference 16 that blade slap may have been present. Remarks made in reference 16 included the comments "rough; blades flapping erratically; unsteady flight." Some characteristics of the SPL versus harmonic plot for this steep descent flight case are different than for either the hover or the forward flight cases. While the maximum SPL value is about the same as for the hover case, and also occurs at the first main rotor harmonic, the second and higher harmonics have SPL values about 10dB higher on the average. The inclusion of vortex street noise increased the SPL values above the fourth harmonic. This increase is on the order of twenty to thirty dB, which is the same order of magnitude increase as was observed for the hover case. An unusual feature of this SPL versus harmonic number curve is the relatively uniform level of noise for the vortex street plus rotational noise above the eighth harmonic. This may be an indication of strong vortex shedding over a wide portion of the blades, with a resulting uniform SPL over a wide frequency range.

Figure 14 shows SPL versus harmonic number for the H-34 helicopter at V = 115 knots. The rotational noise alone is significantly higher than for hover flight condition, and the addition of vortex noise does not give as large an increase in noise level as it did in hover. The inclusion of vortex noise has the greatest effect above the eighth main rotor harmonic, and as in the hover case, inclusion of vortex street noise in addition to rotational noise generally increases the SPL values in the higher harmonics,

and leaves the lower harmonics unaffected. Both the higher level for the rotational noise only, and the increased values of SPL in the higher harmonics are expected results for high forward speed flight conditions as compared to hover flight conditions.

To investigate the effect on the noise characteristics of a blade experiencing impulsive loading, as occurs when a blade passes through or near a trailed vortex, the azimuthal variation of aerodynamic section loading was modified by the same modification as used in reference 9. The results of these calculations are presented in figure 15.

The modified aerodynamic section loading, ASL, is the type suggested in reference 11 to account for an impulsive downwash. The modification was made in the azimuth angle range of approximately 80 degrees to 120 degrees and for fractional blade spans of $r/R = 0.85$, 0.90, and 0.95. The plot of the modified ASL versus azimuth, shown as an insert on figure 15, is for $r/R = 0.95$. The curves for other r/R are included in figure 39 of reference 9. It is noted by comparison of results presented in figures 14 and 15 that no significant difference was obtained in the plots of SPL versus harmonic number as a result of the modification in the ASL Only one set of K_L and K_D values are shown in figures 12 through 15. Other values were used, with the same result as for hover. That is, larger values of K_L and K_D give larger SPL values. Exceptions may occur where cancellation is almost complete at some harmonic numbers for some combinations of K_L and K_D.

Part of the motivation for computing SPL versus harmonic number calculations with the modified ASL for the V = 115 knot case was to determine if noise characteristics which might be indicative of impulsive blade loading could be observed. Such loading is thought to be an important factor in noise characteristics called "slap" or "bang." As may be seen from figure 16, the SPL versus harmonic number plots for rotational noise only differ slightly for the modified and unmodified ASL, for V = 115 knots, and slap or bang noise characteristics are not obvious from this form of noise data presentation. It is noted that noise characteristics generally associated with impulsive blade loading have been identified from experimental pressure time histories rather than plots of SPL versus frequency. Predicted pressure time histories were computed, therefore, for several flight conditions to determine if the distinctive characteristics related to impulsive blade loading could be predicted. Pressure time histories were computed for the H-34 in high speed forward flight with and without modified airload data, for the H-34 in steep descent, and for the HU-1A and H-34 in hover. The high speed forward flight case was done to see if any significant differences in the pressure time histories would be obtained when the measured azimuthal variation of the airloads was modified. The steep descent case was done to see if any indication of blade slap could be observed from the predicted pressure

time history. Since measured time histories were available for the H-34 and HU-1A in hover, predicted time histories for these ships in the same flight condition were obtained. The measured time histories for the H-34 and HU-1A are shown in figures 17 and 18 and predicted time histories for the HU-1A without and with vortex noise effects included are shown in figure 19 and figures 20 and 21, respectively. The pressure time history for the H-34 with vortex noise effects included is shown in figure 22. There are limitations on both the measured and the predicted pressure time histories which seriously restrict any attempt for comparison between them. Some of the limitations are as follows:

1. As previously noted, the instrumentation has a low frequency cut-off which affects frequencies in the range of the first or second harmonic of blade passage. The predicted noise for both the HU-1A and H-34 has its largest component in the first harmonic. Because of the low frequency cut-off, noise at these frequencies does not appear in the measured pressure time histories.

2. The measured noise has significant frequency content above the twentieth harmonic of blade passage frequency, which is the present upper limit on harmonic number for the computer program.

3. The measured noise for the HU-1A contains a large amount of tail rotor noise and the engine exhaust noise is predominant in the H-34 data. The predicted noise, however, contains only main rotor noise.

4. There is no correlation between rotor position and noise measurement at the field point, so the time axis origin cannot be established for comparative purposes.

5. The measured airloads used to compute the time histories were obtained during a different set of flights than those during which the noise measurements were made.

Because of these severe limitations, a comparison of predicted and measured pressure time histories for the helicopters in hover is difficult to accomplish, and has not been attempted.

On the basis of just theoretical results, however, interesting effects may be observed from the predicted pressure time histories. There is a definite similarity in the shapes of the pressure time histories for the HU-1A at field points at seven o'clock ($\psi_0 = 330°$) and eleven o'clock ($\psi_0 = 210°$) as shown in figures 20 and 21, respectively, in that one large pressure pulse occurs in each period. It is noted that the time of arrival of the sharp pressure rise is observed at seven o'clock 0.39T later than at eleven o'clock. The

noted difference in time of arrival would be observed if there were a causative airload characteristic at a single point on the rotor disc located about 42 feet closer to the eleven o'clock field point than to the seven o'clock field point. Two rotor points with that relation to the field point occur near $\psi = 180°$. Inspection of the measured airload data indicates, however, that there is not a distinctive airload variation near these azimuthal locations.

Differences in times of arrival of a pressure time history pattern at different field points could occur for a uniformly loaded rotor. The time shift of the pattern would be proportional to the difference in azimuthal location of the field point, and depends solely on the distance from the blades to the field point. That is, a sound pattern may be thought of as rotating with the helicopter rotor. For the field points in question for a two-bladed rotor rotating counterclockwise, the time shift of the pressure time history would be 2T/3. The predicted pressure time histories do not show agreement with either of the simple models used to explain the possible shift of time of the sound pattern. In reality, both effects will be in operation, and a combination of them will control the pressure time histories over the entire field. (It may be possible to determine the location in the rotor disc of a distinct variation in the airload from the pressure time histories at more than one field point.)

The predicted pressure time history for the H-34 in hover, as shown in figure 22, has a different characteristic than that shown for the HU-1A in that both a positive and a negative pressure peak are apparent for each period. It is noted, however, that the magnitudes of the pressure pulses are approximately the same as that predicted for the HU-1A.

Pressure time histories were plotted for the H-34 helicopter in high speed forward flight without and with theoretically based modifications to the measured airloads. Pressure time histories were plotted for these airloads with rotational noise only in figure 23 (corresponding plots of SPL versus harmonic number were presented in figure 16). As can be seen in figure 23, the modified airload results in a p(t) with a much steeper gradient at about 0.5T than does the unmodified airload. Steep pressure gradients have been associated with the noise caused by interaction of a blade with a trailing tip vortex of a preceding blade. As previously noted, this distinctive change in noise characteristic was not observed in the plot of SPL versus harmonic number for the modified airloads.

Figures 24 and 25 show the pressure time histories as computed for the H-34 in high speed flight including the combined rotational and vortex street airloads. Figure 24 presents the predicted time histories for the unmodified airloads and figure 25 presents the

results using the modified airloads. The pressure time histories for the high forward speed cases are significantly changed by the addition of vortex street noise. Superposition of sound from the rotational and vortex street forces occurs, so large magnitude high frequency components, which come from the vortex noise, tend to mask the steep gardient observed in the pressure time history from the modified airload data with rotational noise only, as was shown in figure 23. It is interesting to note in comparing the results of figures 24 and 25 that the combined vortex and rotational noise seemed to concentrate the high frequency oscillations due to vortex shedding over a narrow azimuth range when the modified airloads were used. The high frequency content, however, is present over a majority of the time periods for the unmodified airload case. High frequency variation of sound pressure over a narrow azimuth band has been associated with blade slap (ref. 7) as caused by blade-vortex interaction.

The pressure time history for the steep descent case, presented in figure 26, also has large magnitude high frequency variations over a limited portion of the period. The large magnitude high frequency noise comes from vortex shedding and as may be seen from the plot of SPL versus harmonic number in figure 15, the vortex noise is dominant in the high harmonics. As previously noted, the combination of large magnitude high frequency noise over a limited ψ range has been identified as blade slap. It is noted, however, in reference 7 that the frequency content is significantly higher than that shown in figure 26. This difference is believed to be caused by the fact that the upper limit on frequency of the present computer program is the twentieth harmonic of blade passage. The nondimensional time period over which the observer receives this high frequency noise corresponds to a blade-vortex interaction occurring near the 90° azimuthal location of the rotor disc, which is not an unusual location for this phenomenon to occur.

An important conclusion that can be drawn from the results obtained during the analysis of the high speed forward flight and steep descent cases is that important noise characteristics, such as blade slap, are shown from plots of pressure time history which are not recognizable from the usual plots of SPL versus harmonic number.

CONCLUDING REMARKS

The theory for calculating helicopter rotor noise has been extended to include vortex street shedding noise as a noise source in addition to rotational noise. A numerical integration was used to evaluate the sound pressure levels and pressure time histories for up to 20 harmonics of the main rotor blade at a general field point translating with the hub.

Vortex street force magnitude constants were determined by a least squares fit approach using the difference between the total measured noise and the predicted rotational noise for the HU-1A helicopter in hover. While it was hoped that these might be "universal constants," the approximations involved in predicting the magnitude of the rotational noise, and limitations in the measured data results in these values for the vortex street constants being order of magnitude estimates only.

These vortex street constants were, however, used to predict sound pressure levels and pressure time histories for the HU-1A helicopter in hover and for the H-34 helicopter in various flight conditions. Results showed that (for hover, high forward speed, and steep descent) the first four or five harmonics are the largest and are unaffected by the vortex noise. Higher harmonic levels do appear to have significant vortex noise, so that application of this new theory resulted in an appreciable improvement between predicted and measured sound pressure levels. It is noted, however, that with the addition of the vortex shedding effects, the increase in the noise levels at the higher harmonics for the hover and the steep descent flight conditions was approximately twice that determined for the high forward speed case.

While a significant improvement in predicted noise was achieved, noise levels at harmonics of the blade passage frequency still were not accurately predicted. This may be due to deficiencies in the theory, or it may be due to deficiencies in the experimental airload data required for the calculation of the higher harmonics of the rotational noise. Since the vortex noise occurs over a wide range of frequencies rather than only at the discrete frequencies of rotational noise, the level of the vortex noise is that of the off-harmonic noise, and significant changes in the isolated harmonic peaks should not be expected from the vortex noise. While the forces associated with thickness effects and vortex shedding are relatively small, it is noted that high frequency forces of relatively small magnitude can make a significant contribution to the rotor noise in the higher frequency range, regardless of their origin.

Predicted sound pressure time histories were presented for various flight conditions. Results of these theoretical calculations indicate that blade slap characteristics may be observed from predicted pressure time histories for both high forward speed and steep descent flight conditions, but will probably not be recognizable from the corresponding plots of sound pressure levels versus harmonic number.

Based on the research effort reported herein the following specific comments are presented.

1. The experimentally determined sound pressure level data for hover flight condition which was used for correlation shows that the off-harmonic peaks are the same order of magnitude as the harmonic peaks, in the higher harmonics.

2. Vortex noise is a significant noise source in all flight conditions but is more pronounced in hover and steep descent flight conditions.

3. Use of the same nondimensional constants describing the frequency and force characteristics of vortex shedding for two different helicopter rotor systems produced comparable improvement in the prediction of the rotor noise in the high frequency range.

4. Rotational noise alone, even that associated with a rapid change in airloading, does not yield a pressure time history similar to that measured for blade slap (high frequency high amplitude noise over a limited portion of a blade passage time period).

5. The inclusion of both vortex and rotational noise effects yields a pressure time history similar to that associated with blade slap for high forward speed and steep descent flight conditions.

6. Published measured airload data is currently inadequate for use in predicting the higher harmonics of rotational noise.

7. It is considered unlikely that theoretical methods can be developed to accurately predict the required harmonic airloads in the harmonic range of 10 through 100.

REFERENCES

1. Loewy, Robert G.: Aural Detection of Helicopters in Tactical Situations. J. Am. Helicopter Soc., vol. 8, no. 4, Oct. 1963. pp. 36-53.
2. Sternfeld, Harry, Jr.; and Forehand, J. Everette: Helicopter Noise, Its Evaluation and Treatment. Proceedings of the American Helicopter Society Seventeenth Annual Forum, Washington, D.C., May 3-5, 1961.
3. Gutin, L.: On the Sound Field of a Rotating Propeller. NACA TM 1195, 1948.
4. Deming, Arthur F.: Propeller Rotation Noise Due to Torque and Thrust. NACA TN 747, 1940.
5. Garrick, I.E.; and Watkins, C.E.: A Theoretical Study of the Effect of Forward Speed on the Free-Space Sound-Pressure Field Around Propellers. NACA TN 3018, 1953.
6. Spencer, R.H.; H. Sternfeld, Jr.; and McCormick B.W.: Tip Vortex Core Thickening for Application to Helicopter Rotor Noise Reductions. USAAVLABS Tech. Report 66-1, Sept. 1966.
7. Anon: A Study of the Origin and Means of Reducing Helicopter Noise. TCREC Tech. Report 62-73, Nov. 1962.
8. Schlegel, Robert; King, Robert; and Mull, Harold: Helicopter Rotor Noise Generation and Propagation. USAAVLABS Tech. Report 66-4, Oct. 1966.
9. Loewy, R.G. and Sutton, L.R.: A Theory for Predicting the Rotational Noise of Lifting Rotors in Forward Flight, Including a Comparison with Experiment. USAAVLABS Tech. Report 65-82, Jan. 1966.
10. Lowson, M.V.: Basic Mechanisms of Noise generation by Helicopters, V/STOL Aircraft, and Ground Effect Machines. Wyle Laboratories Report No. WR65-9, May 1965.
11. Yudin, E.Y.: On the Vortex Sound from Rotating Rods. NACA TM 1136. 1947.
12. Miller, R.H.: On the Computation of Airloads Acting on Rotor Blades in Forward Flight. J. Am. Helicopter Soc. vol. 7, no. 2, Apr. 1962, pp. 56-66.
13. Piziali, R.A.; and DuWaldt, F.A.: A Method for Computing Rotary Wind Airload Distributions in Forward Flight. TCREC TR 62-44, Nov. 1962.
14. Gessow, A.; and Myers, G.C.: Aerodynamics of the Helicopter. MacMillan Company, 1952.
15. Nikolsky, A.A.: Helicopter Analysis. John Wiley and Sons, Inc. 1951.
16. Scheiman, James: A Tabulation of Helicopter Rotor-Blade Differential Pressures, Stresses, and Motions as Measured in Flight. NASA TM X-952, 1964.
17. Anon: Measurement of Dynamic Air Loads on a Full-Scale Semi-rigid Rotor. TCREC Tech. Report 62-42, Dec. 1962.

18. Hubbard, H.H.; and Regier, A.A.: Propeller-Loudness Charts for Light Airplanes. NACA TN 1358, 1947.
19. Stowell, E.Z.; and Deming, A.F.: Vortex Noise from Rotating Cylindrical Rods. NACA TN 519, 1935.
20. Sharland, I.J.: Sources of Noise in Axial Flow Fans Journal of Sound and Vibration, vol. 1, no. 3, 1964, pp. 302-332.
21. Blokhintsev, D.: Acoustics of a Nonhomogeneous Moving Medium. NACA TM 1399, 1959.
22. Roshko, A.: On the Drag and Shedding Frequencies of Two-dimensional Bluff Bodies. NACA TN 3169, 1954.
23. Bearman, P.W.: On Vortex Street Wakes. National Physical Laboratory Aero Report 1199, (A.R.C. 28 143), 18 Apr. 1966.
24. von Doenhoff, A.E.; and Tetervin, N.: Determination of General Relations for the Behavior of Turbulent Boundary Layers. NACA Rept. 772, 1943.
25. Krzywoblocki, M.Z.: Investigation of the Wing-Wake Frequency with Application of the Strouhal Number. J. Aeron. Sci., vol. 12, no. 1, Jan. 1945, pp. 51-62.
26. Lamb, H.: The Dynamical Theory of Sound. Second ed., Dover, 1960.
27. Etkin, B.; Korbacher, G.K., and Keefe, R.T.: Acoustic Radiation from a Stationary Cylinder in a Fluid Stream (Aeolian Tones). J. Acoust. Soc. Am., vol. 29, no. 1, Jan. 1957, pp. 30-36. (See also vol. 34, no. 11, Nov. 1962, pp. 1711-1714).
28. Foughner, J.T., Jr.; and Duncan, R.L.: A Full-Scale Ground Wind Load Program, Paper presented at the Meeting on Ground Wind Load Problems in Relation to Launch Vehicles. NASA TM X-57779, 1966, pp. 4.1 - 4.19.
29. Lighthill, M.J.: The Bakerian Lecture, 1961, Sound Generated Aerodynamically. Royal Aircraft Establishment Technical Memorandum No. Dir. 8, Nov. 1961.
30. Hubbard, H.H.; and Maglieri, D.J.: Noise Charactertistics of Helicopter Rotors at Tip Speeds up to 900 ft/sec. J. Acoust. Soc. Am., vol. 32, no. 9, Sept. 1960, pp. 1105-1107.
31. Hildebrand, Francis B.: Advanced Calculus for Applications. Prentice - Hall, Inc., 1962.

TABLE I. FIELD POINT MEMBERS AND POSITIONS

Field point member	Field point position			
	vertical distance Z_0	radius R_0	angle ψ_0	('clock' position)
F.P. 1	-11.4 feet	200 feet	330°	(7:00)
F.P. 2	-16.0 feet	200 feet	330°	(7:00)
F.P. 3	-16.0 feet	200 feet	120°	(2:00)
F.P. 4	-56.0 feet	112 feet	90°	(3:00)
F.P. 5	-11.4 feet	200 feet	210°	(11:00)

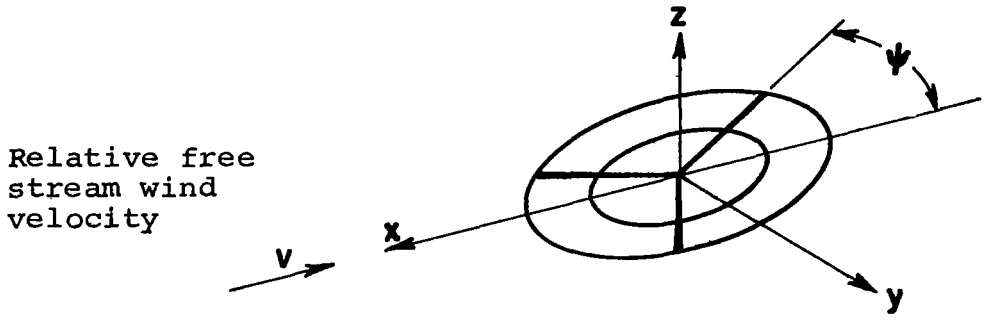

Figure 1. Coordinate system, isometric view.

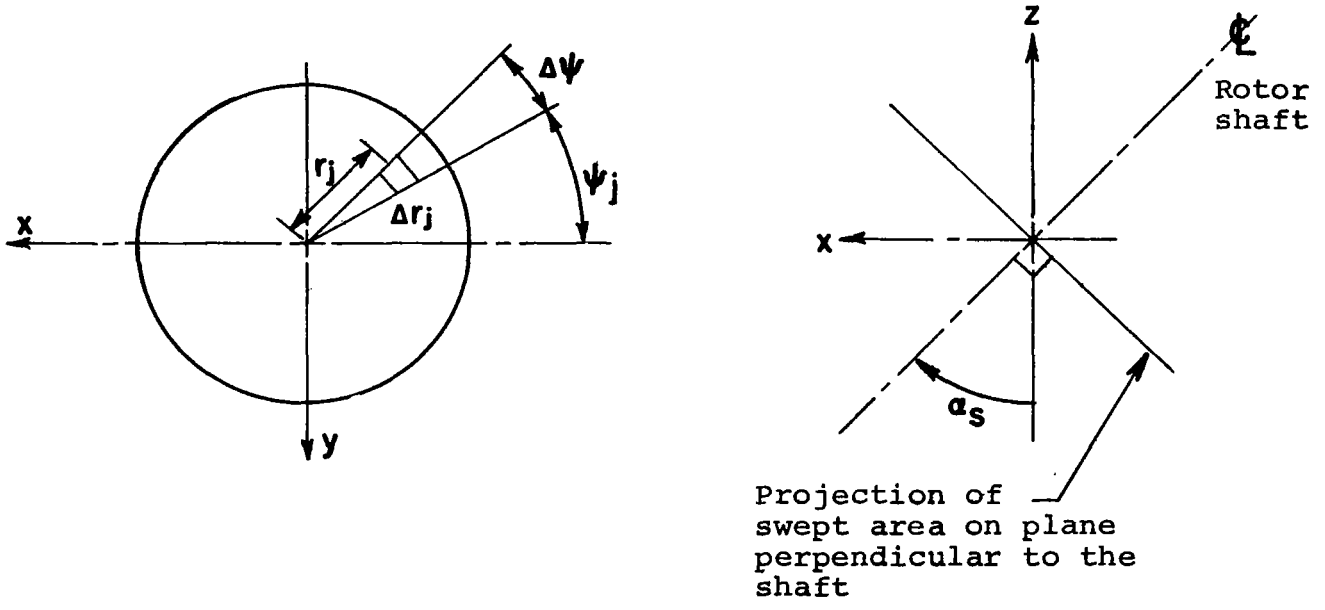

Figure 2. Coordinate system.

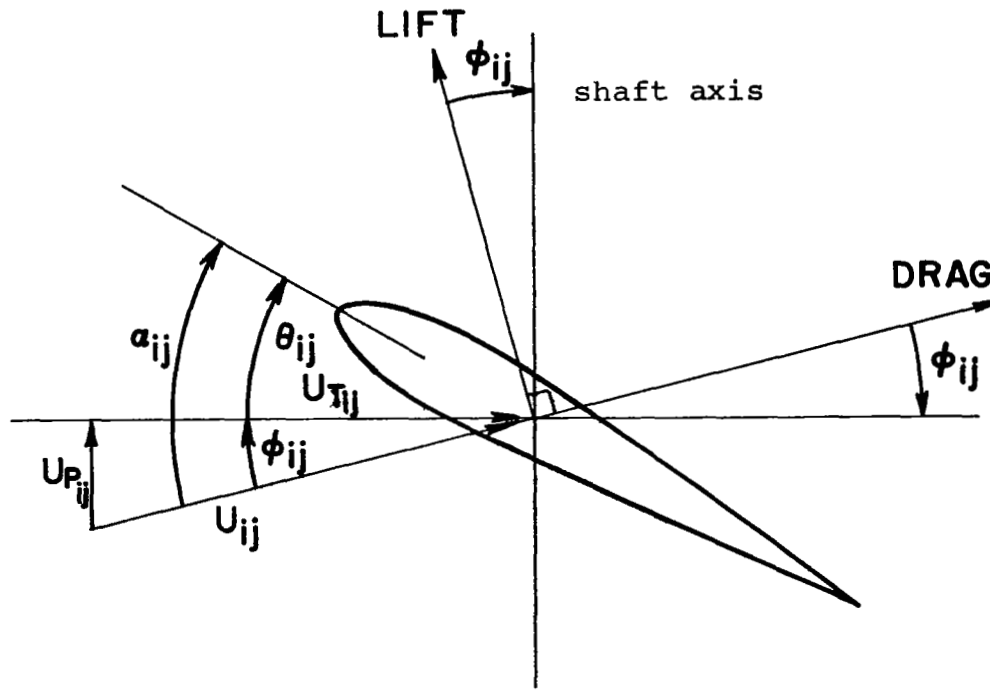

Figure 3. Blade section quantities.

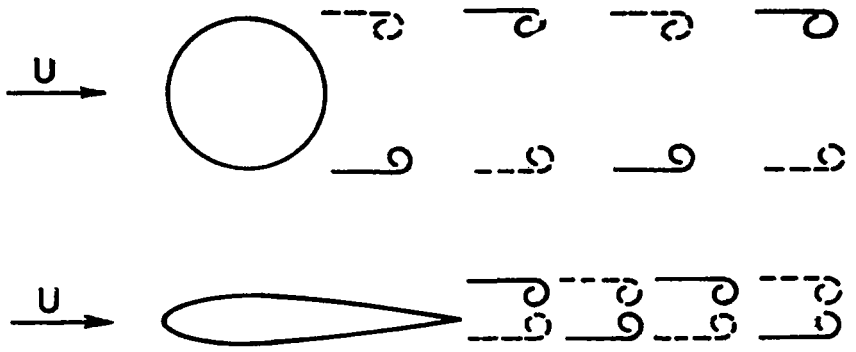

Symmetrical bodies, vortex drag frequency is twice the shedding frequency.

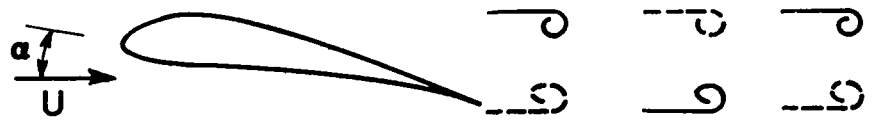

Nonsymmetrical bodies includes vortex drag frequency the same as vortex shedding frequency.

Figure 4. Effect of body symmetry on vortex street drag frequency.

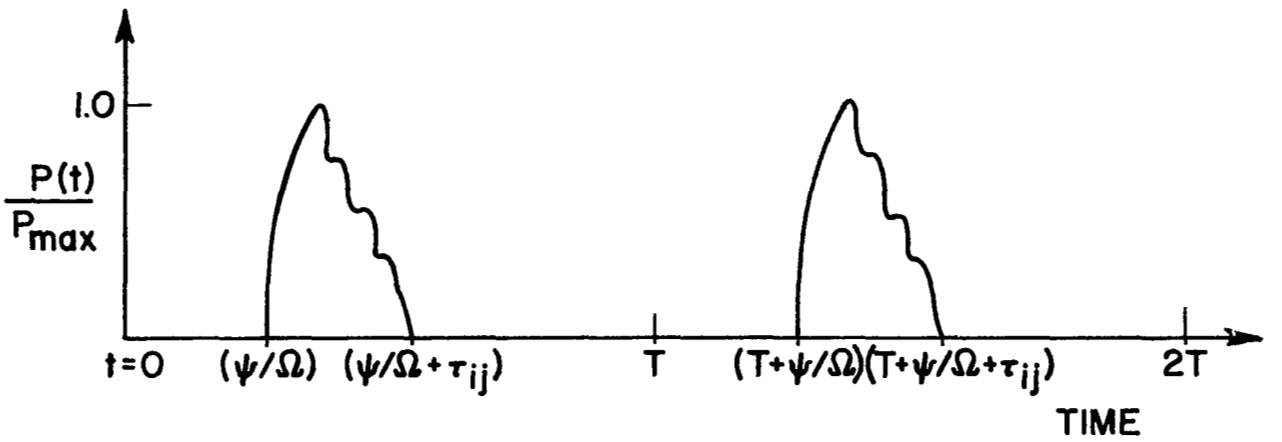

Figure 5. Pressure pulse period.

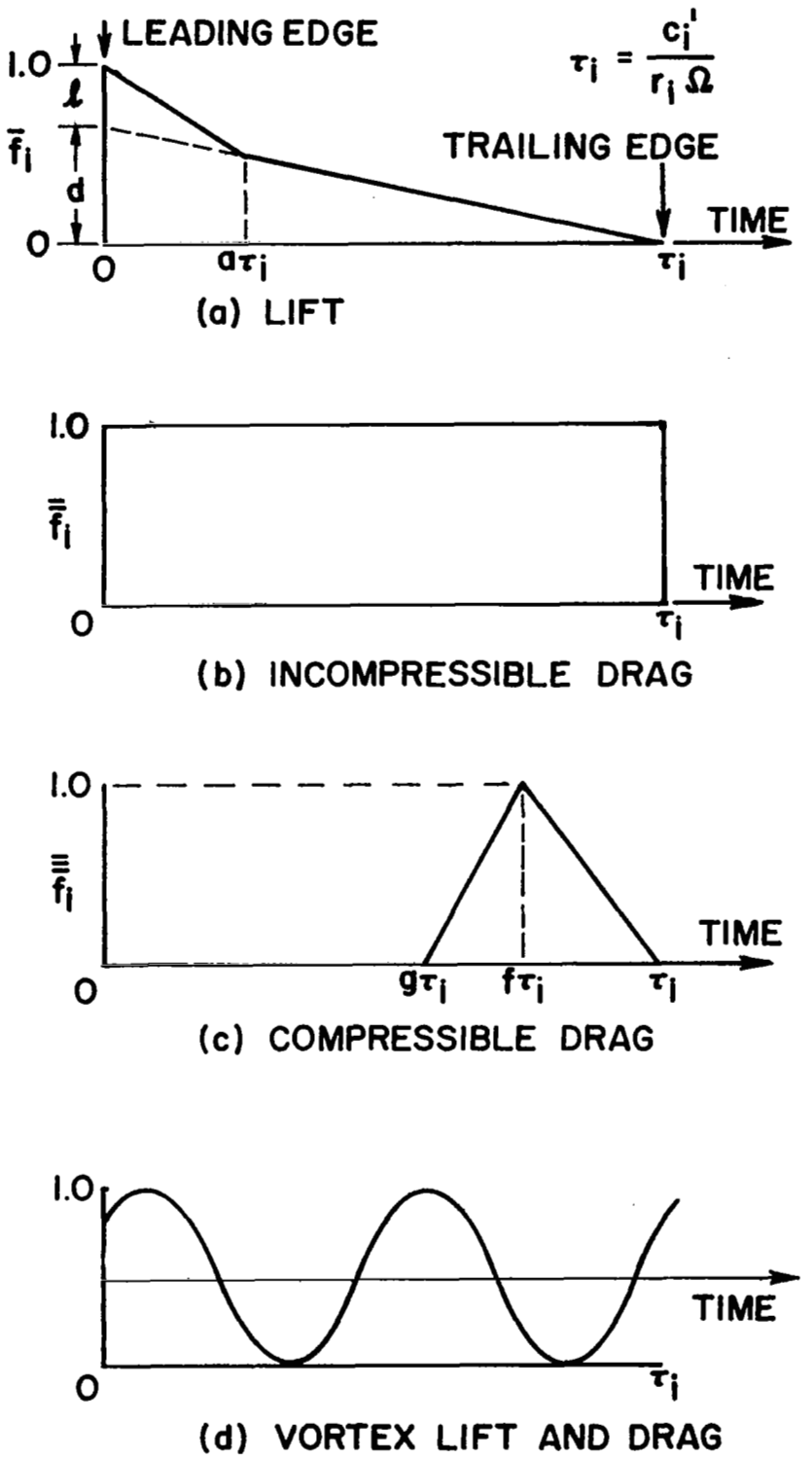

Figure 6. Idealized force distributions versus chord, time.

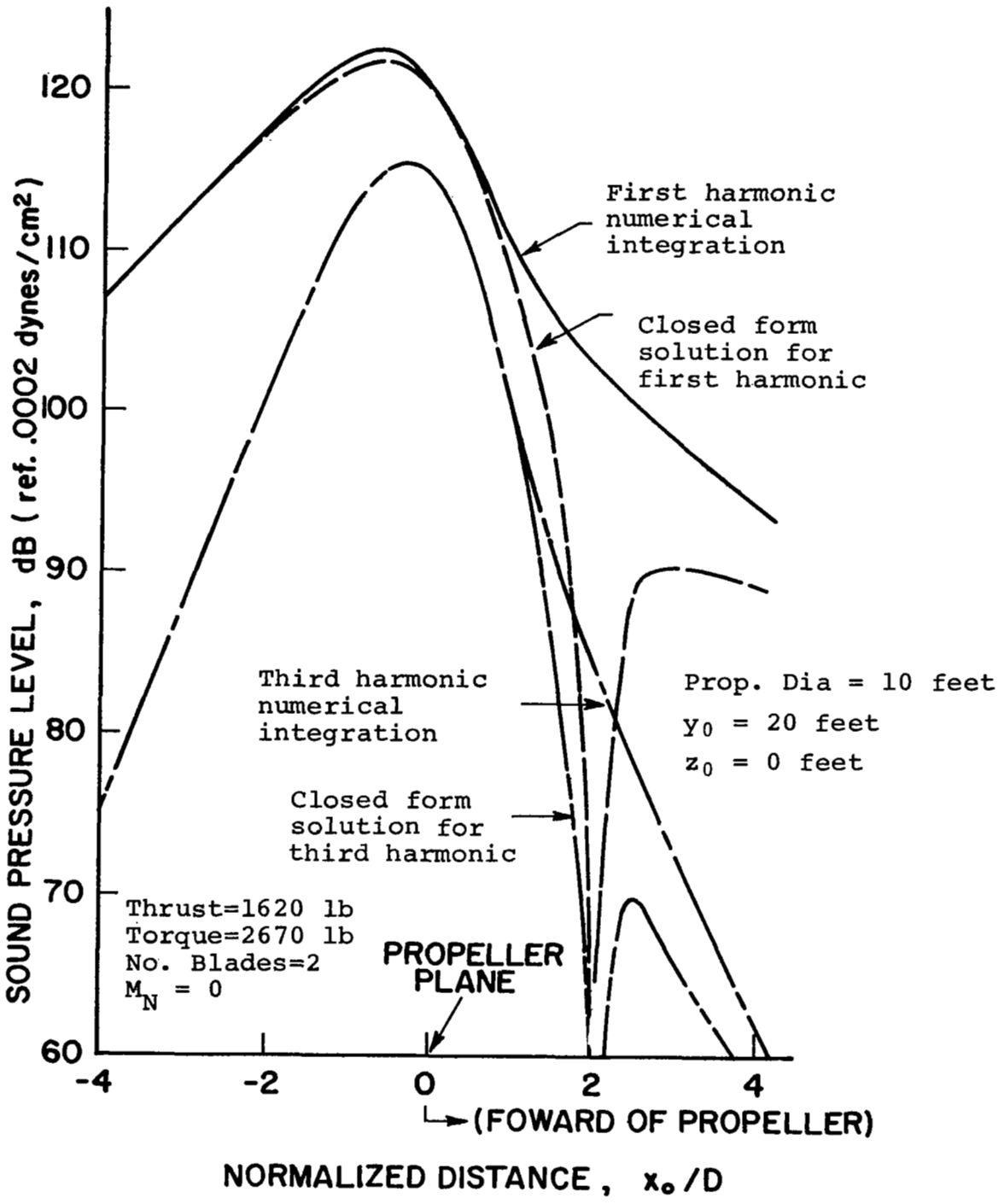

Figure 7. Comparison of predicted noise with and without far field assumption.

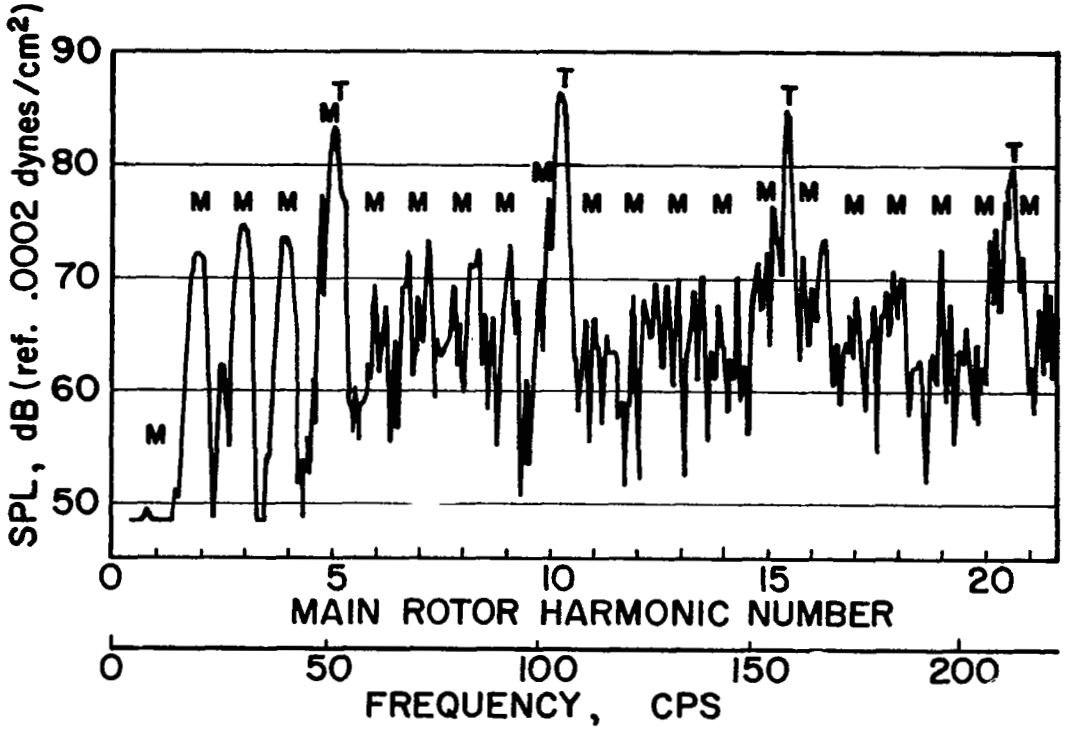

Figure 8. SPL vs frequency for HU-1A helicopter in hover. (Main rotor and tail rotor harmonics are indicated by the letters M and T, respectively.) F.P. 1, 3 cps bandwidth filter.

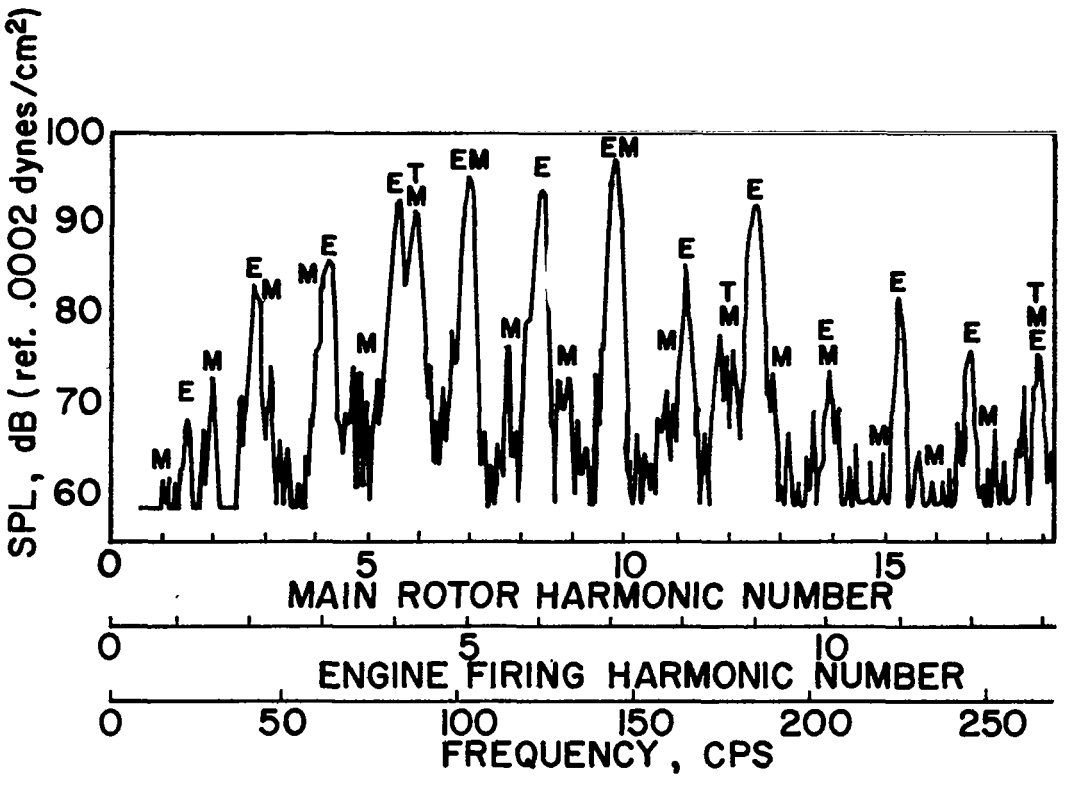

Figure 9. SPL vs frequency for H-34 helicopter in hover. (Engine, main rotor, and tail rotor harmonics are indicated by the letters E, M, and T, respectively.) F.P. 2, 3 cps bandwidth filter.

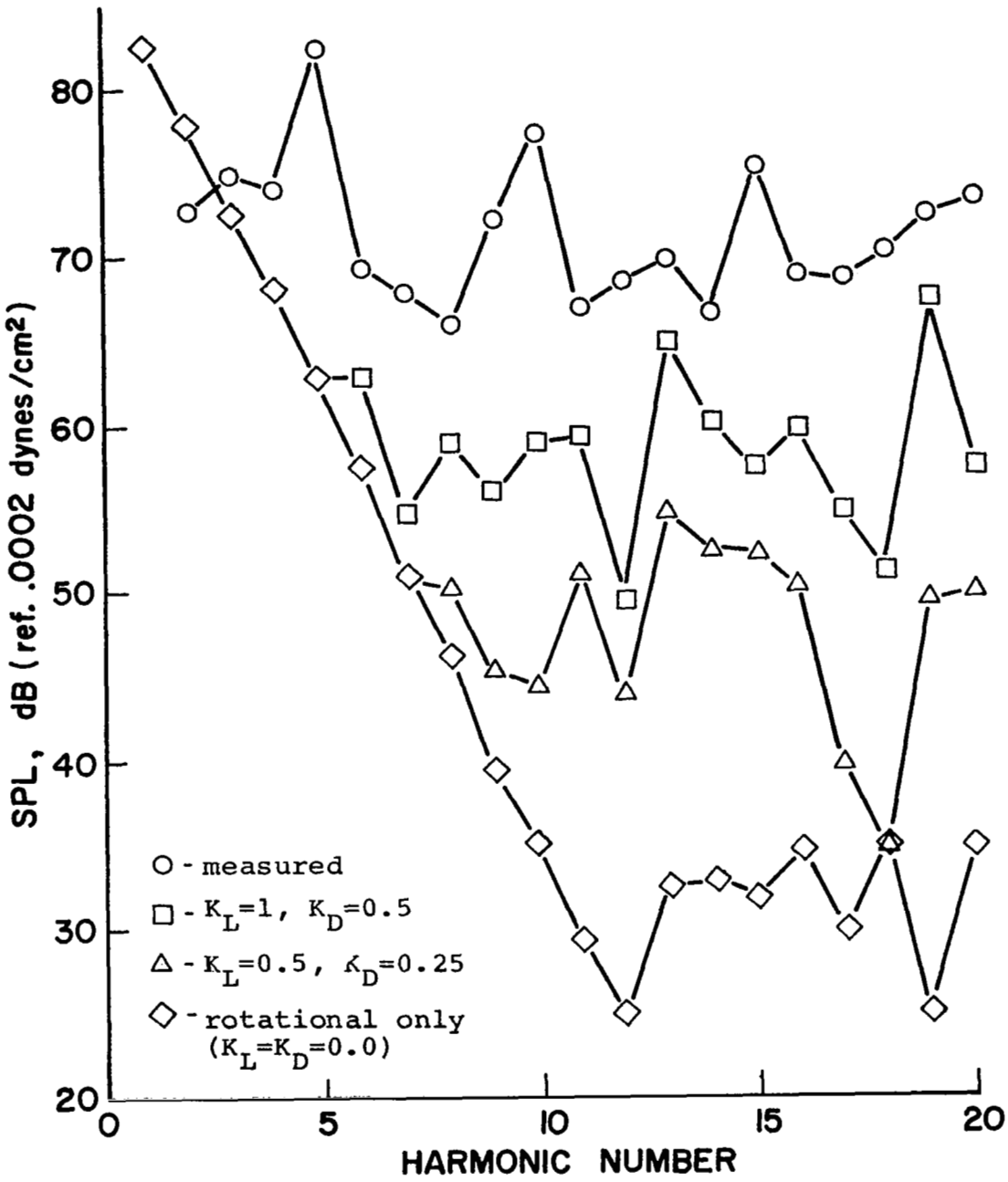

Figure 10. Comparison of computed SPL's vs harmonic number for various K_L and K_D, with measured SPL's. HU-1A helicopter in hover, h/d=1.54, F.P. 1.

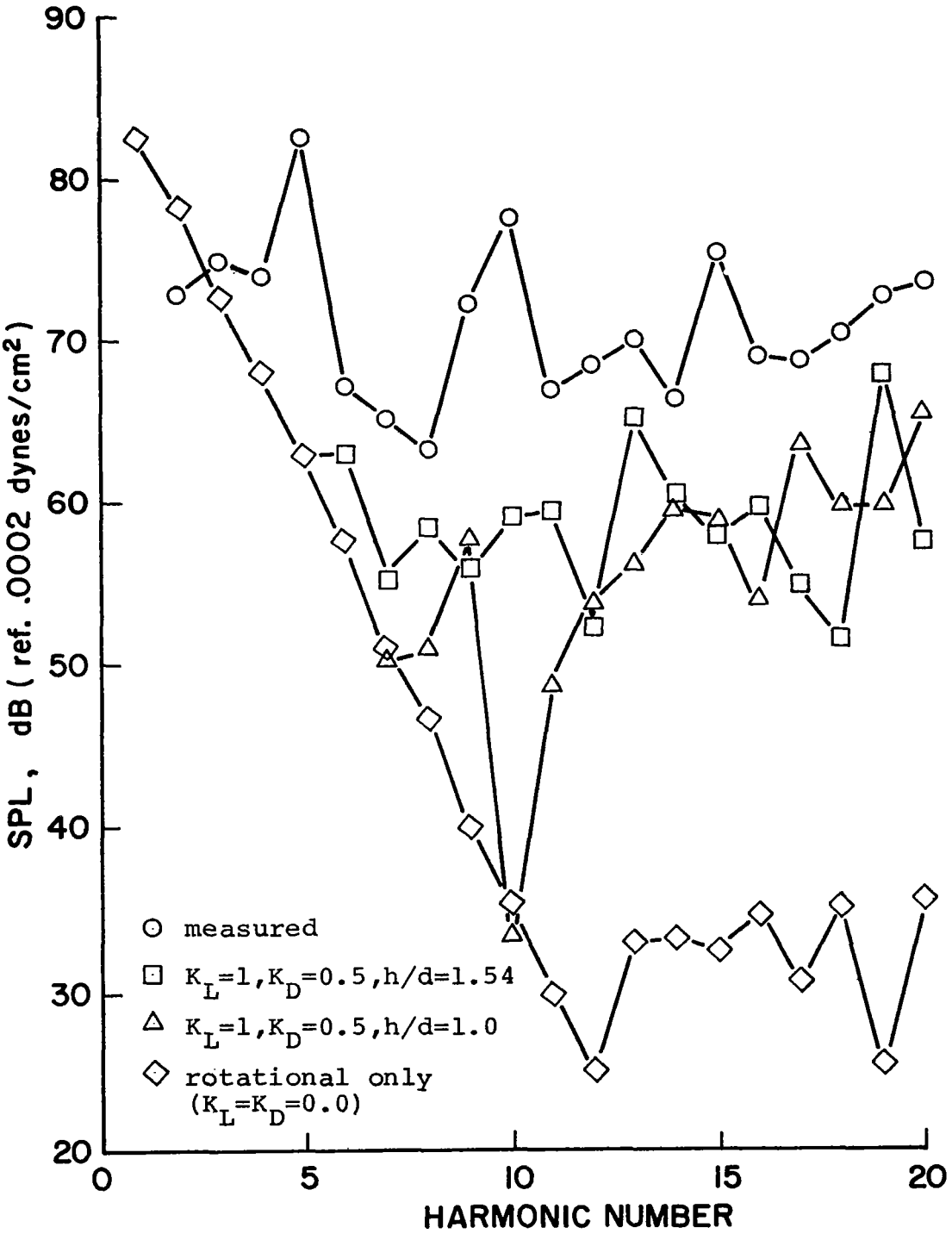

Figure 11. Comparison of computed SPL's vs harmonic number for h/d of 1.0 and 1.54. HU-1A helicopter in hover, F.P. 1.

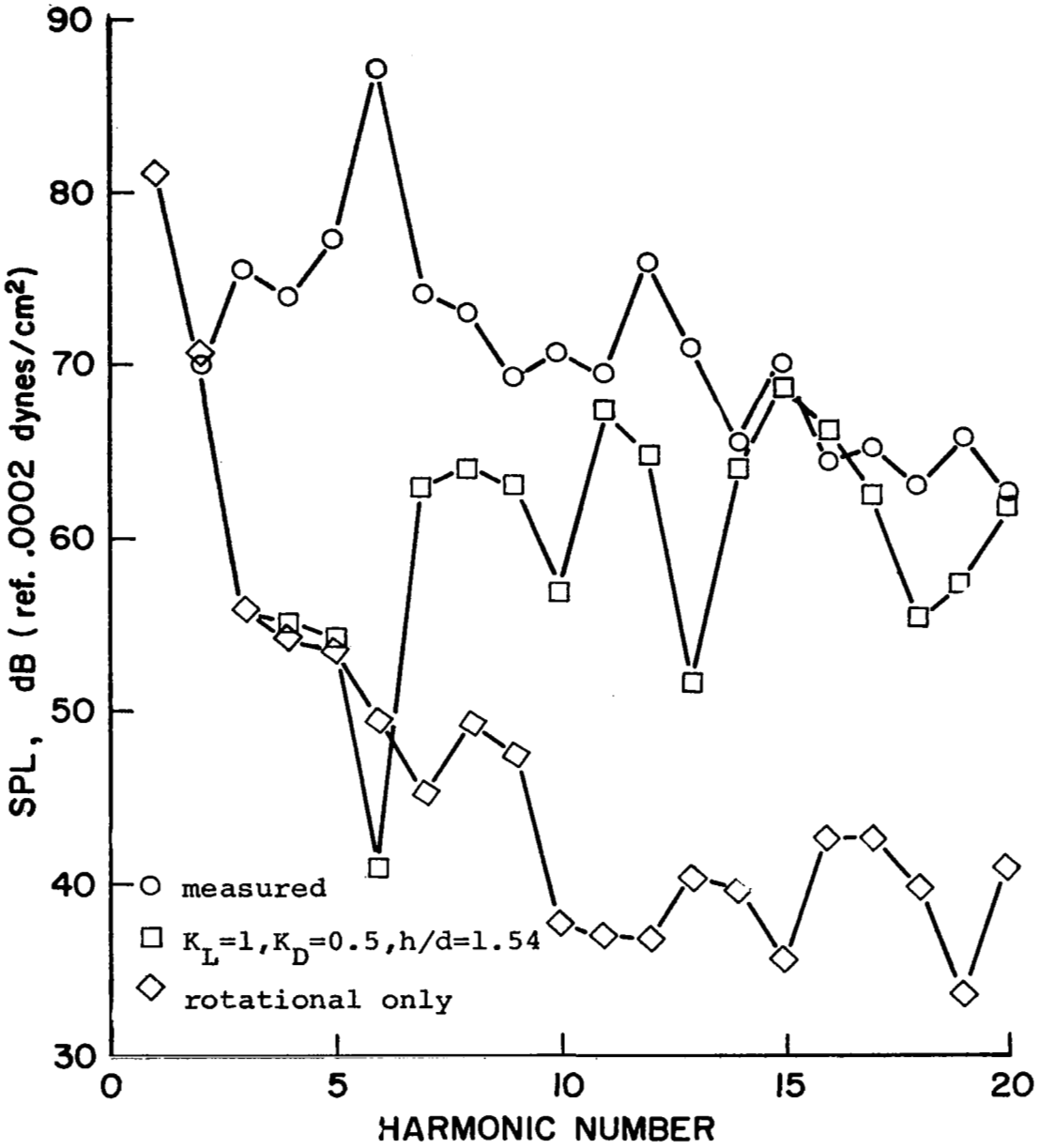

Figure 12. Comparison of computed SPL's vs harmonic number with measured SPL's. H-34 helicopter in hover, F.P. 3.

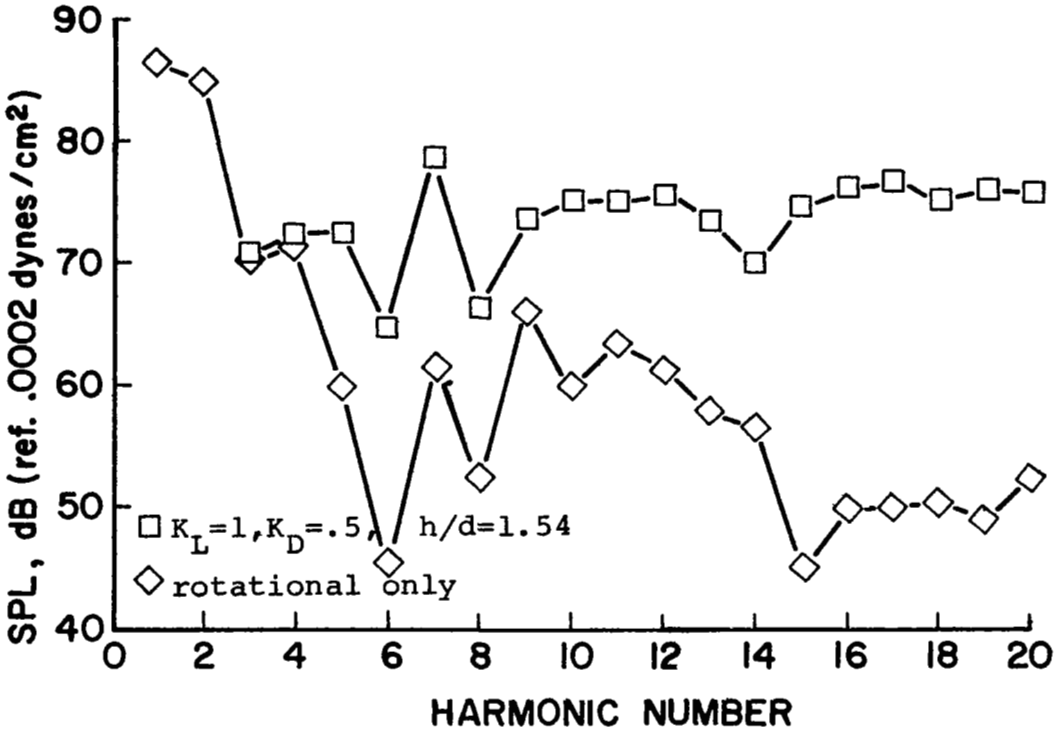

Figure 13. Computed SPL's vs harmonic number for steep descent. H-34 helicopter, $\bar{V} \approx 0$, F.P. 4.

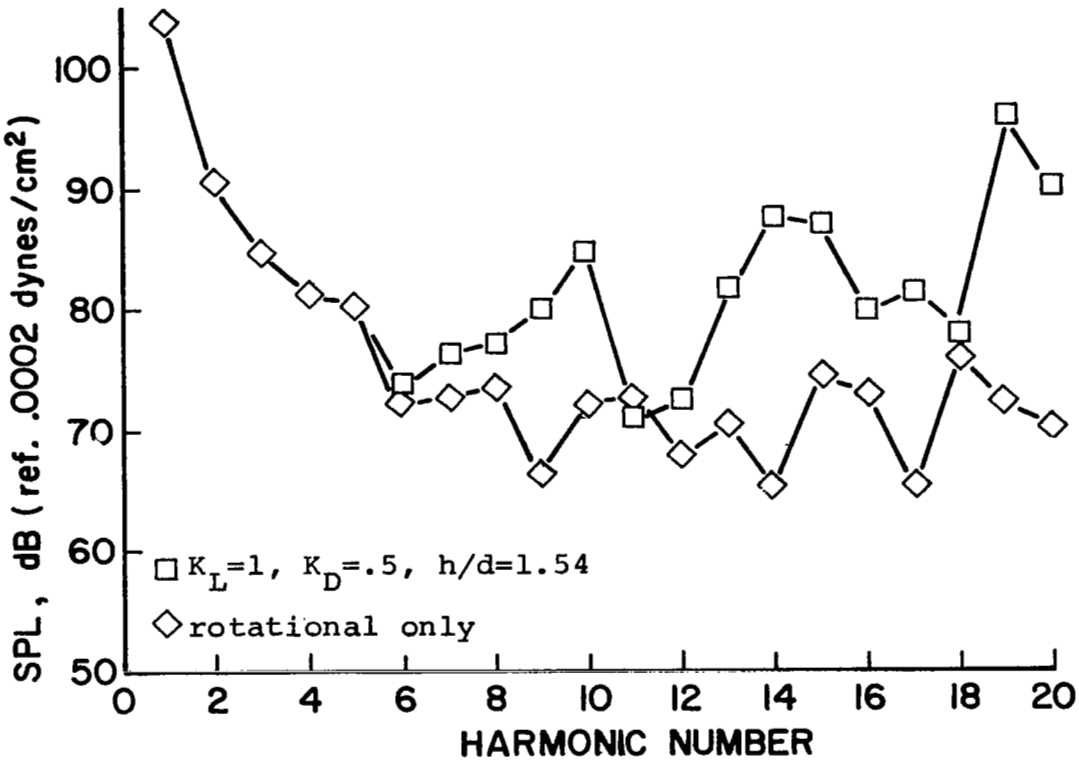

Figure 14. Computed SPL's vs harmonic number from unmodified ASL's. H-34 helicopter, V=115 knots, F.P. 4.

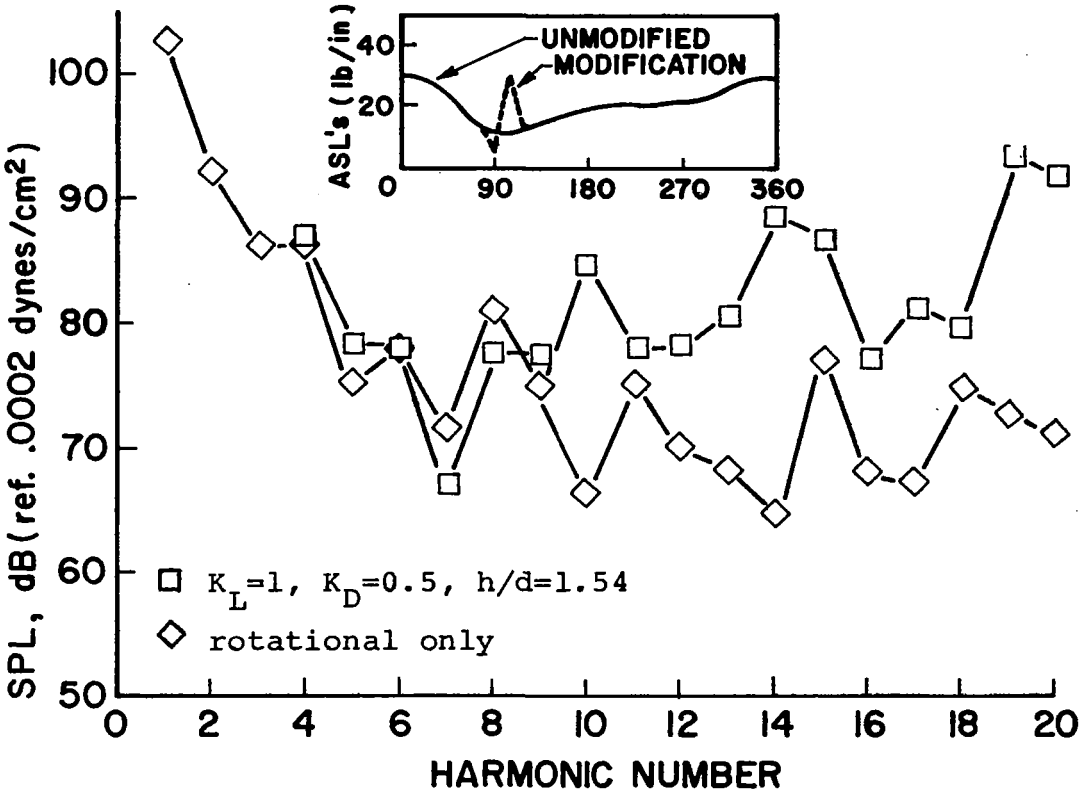

Figure 15. Computed SPL's vs harmonic number from modified ASL's. H-34 helicopter, V = 115 knots, F.P. 4.

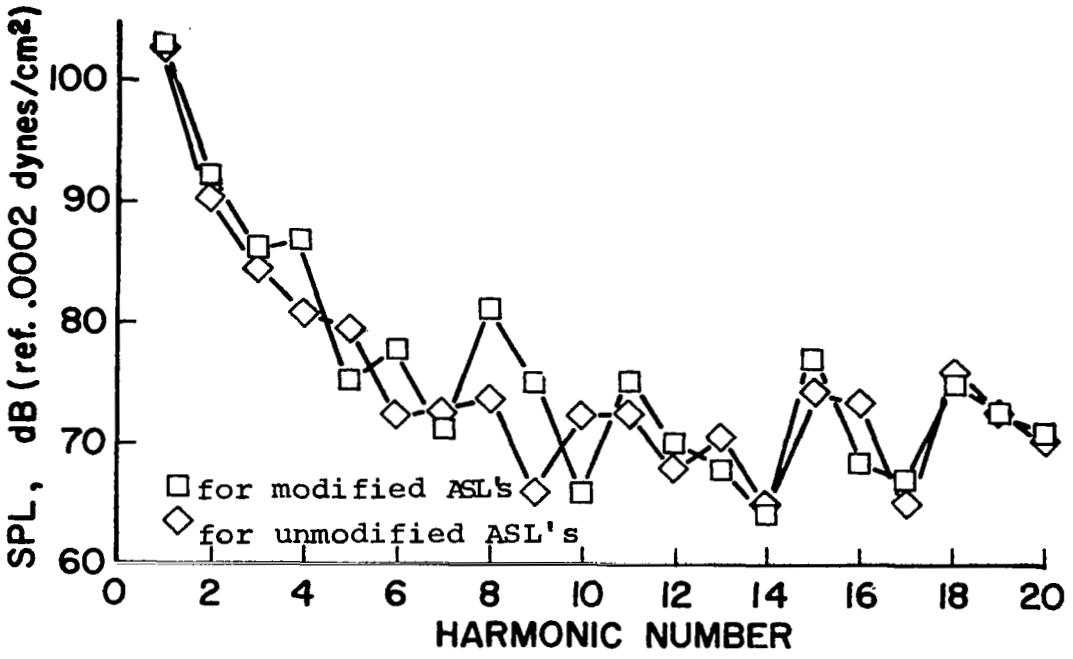

Figure 16. Comparison of computed SPL's vs harmonic number for modified and for unmodified ASL's. H-34 helicopter with rotational noise only, V=115 knots, F.P. 4.

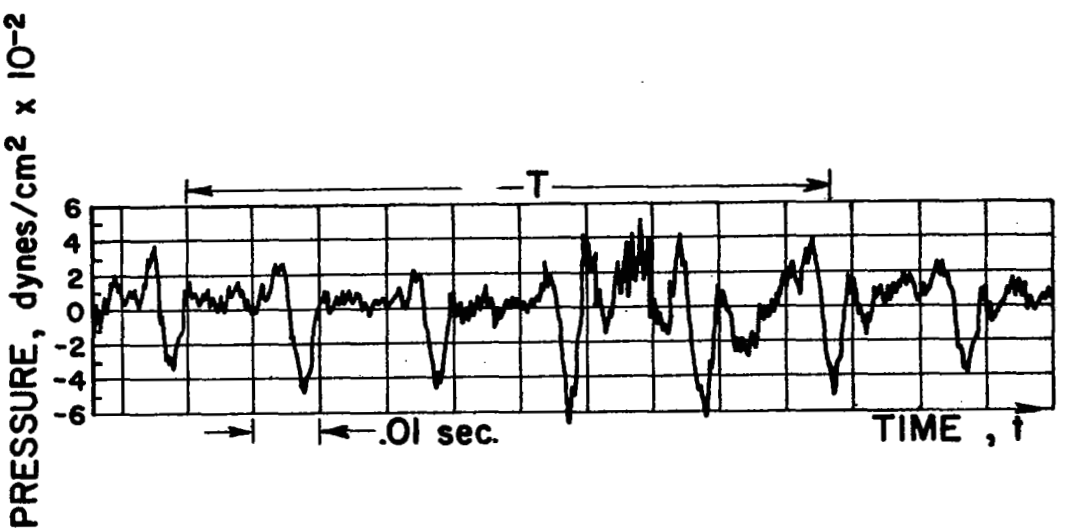

Figure 17. Measured pressure time history for HU-1A helicopter in hover, F.P. 1.

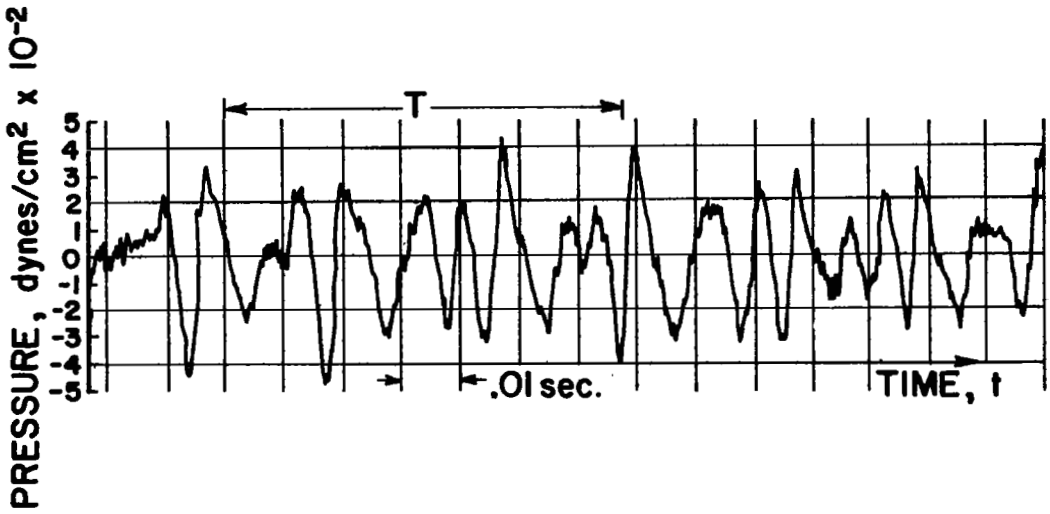

Figure 18. Measured pressure time history for H-34 helicopter in hover, F.P. 2.

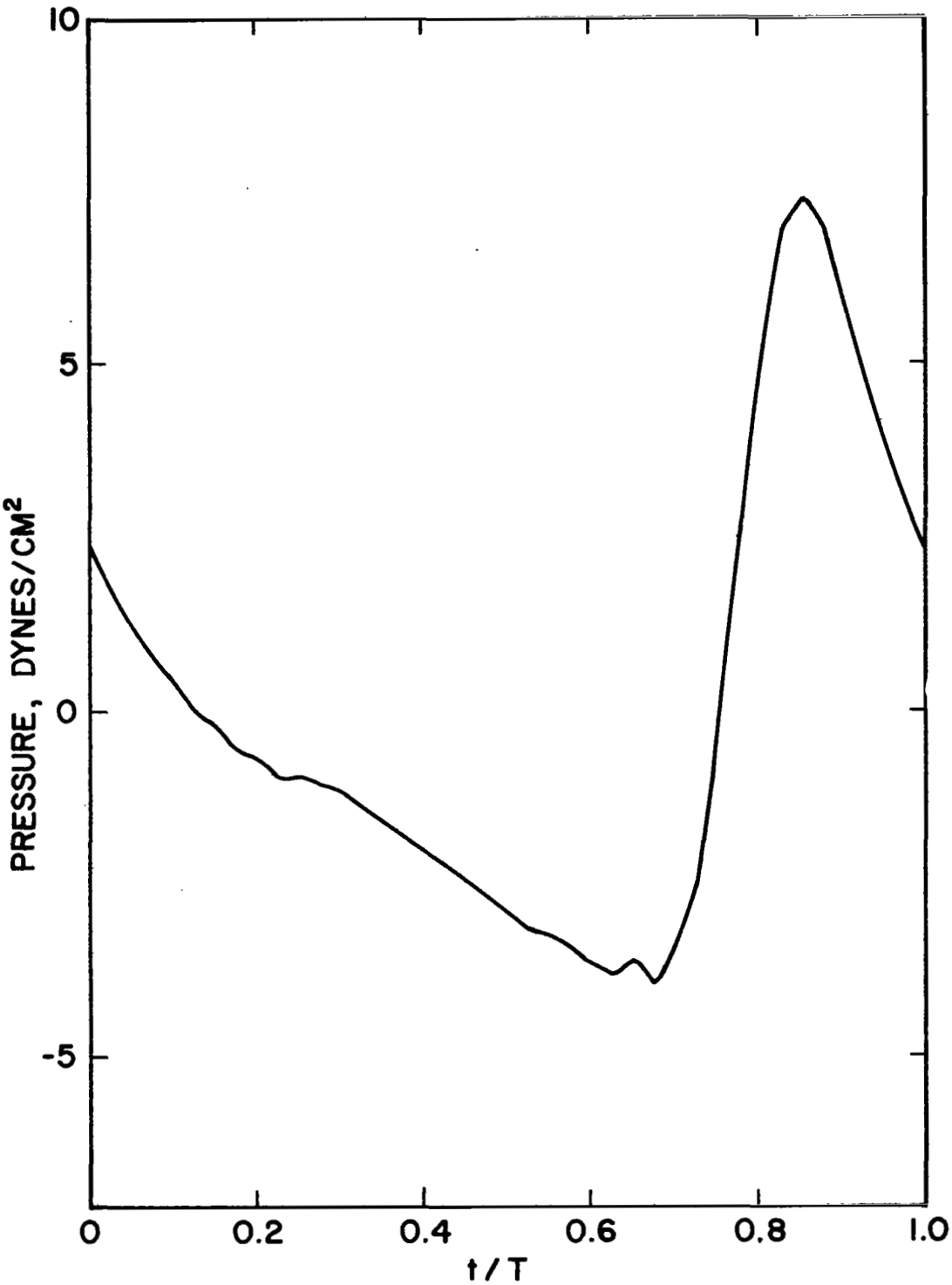

Figure 19. Computed pressure time history with rotational noise only for HU-1A helicopter in hover, F.P. 5.

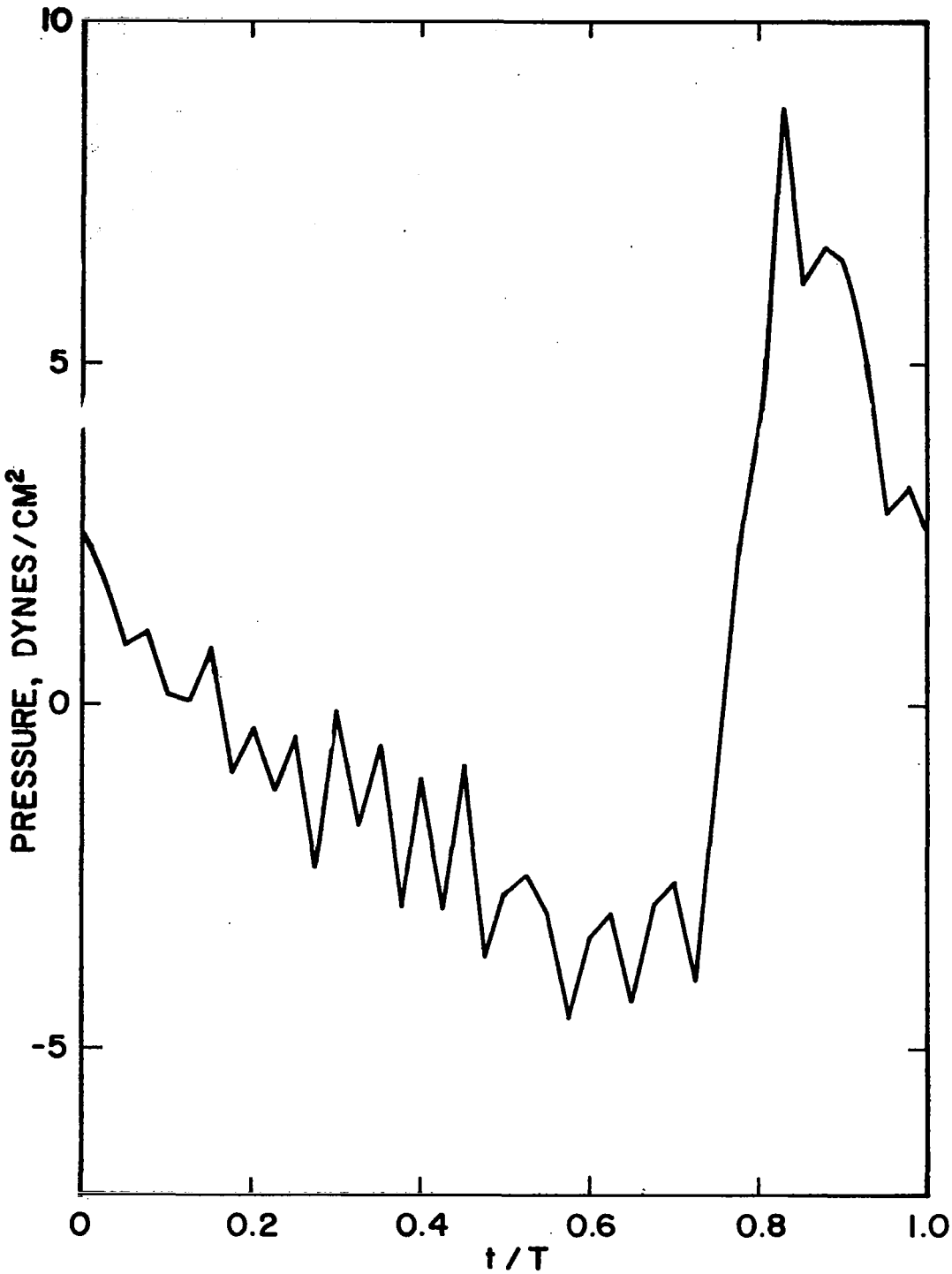

Figure 20. Computed pressure time history with rotational and vortex noise for HU-1A helicopter in hover, K_L=1.0, K_D=0.5, F.P. 5.

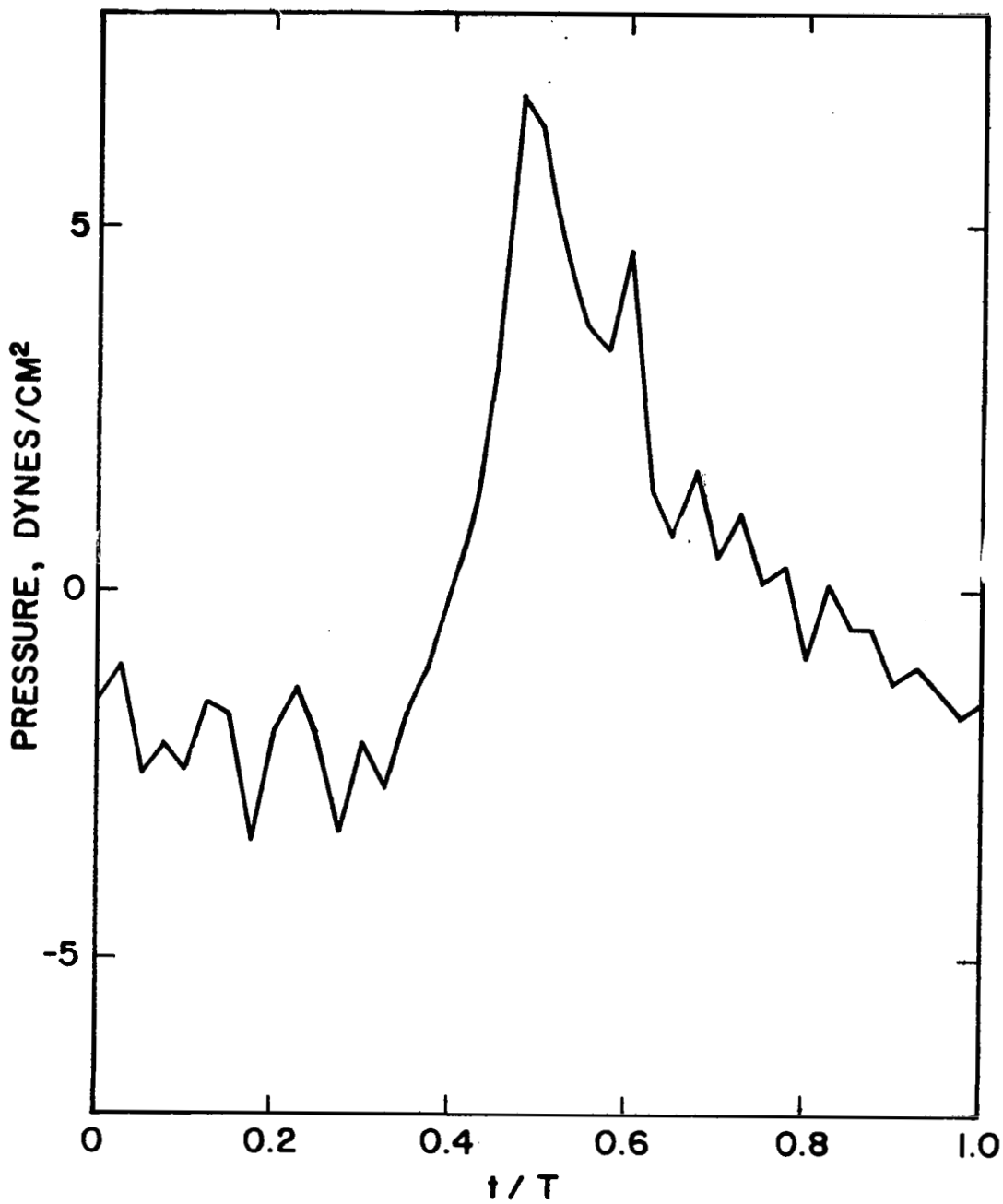

Figure 21. Computed pressure time history with rotational and vortex noise for HU-1A helicopter in hover, K_L=1.0, K_D=0.5, F.P. 1.

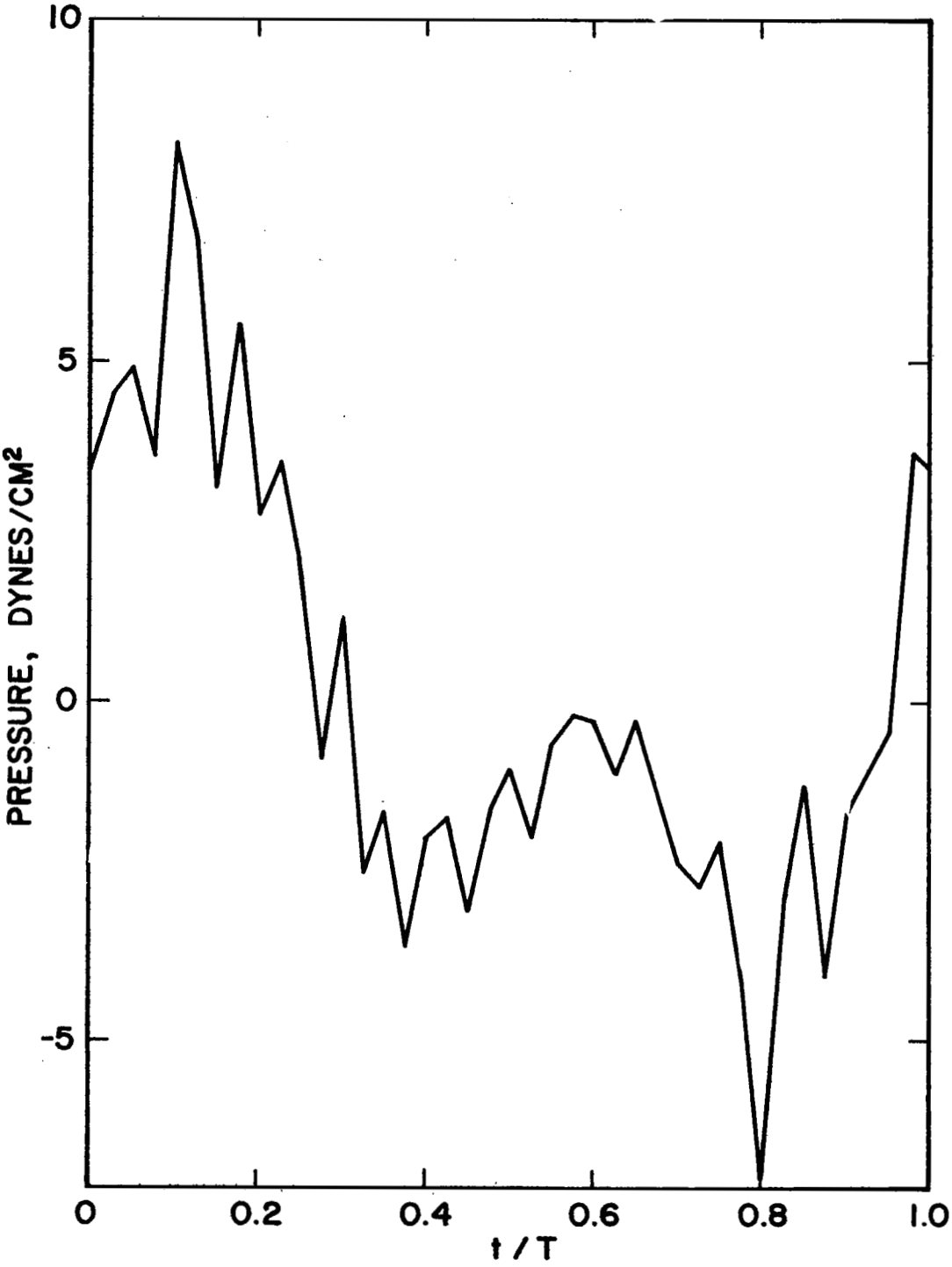

Figure 22. Computed pressure time history with rotational and vortex noise for H-34 helicopter in hover, K_L=1.0, K_D=0.5, F.P. 3.

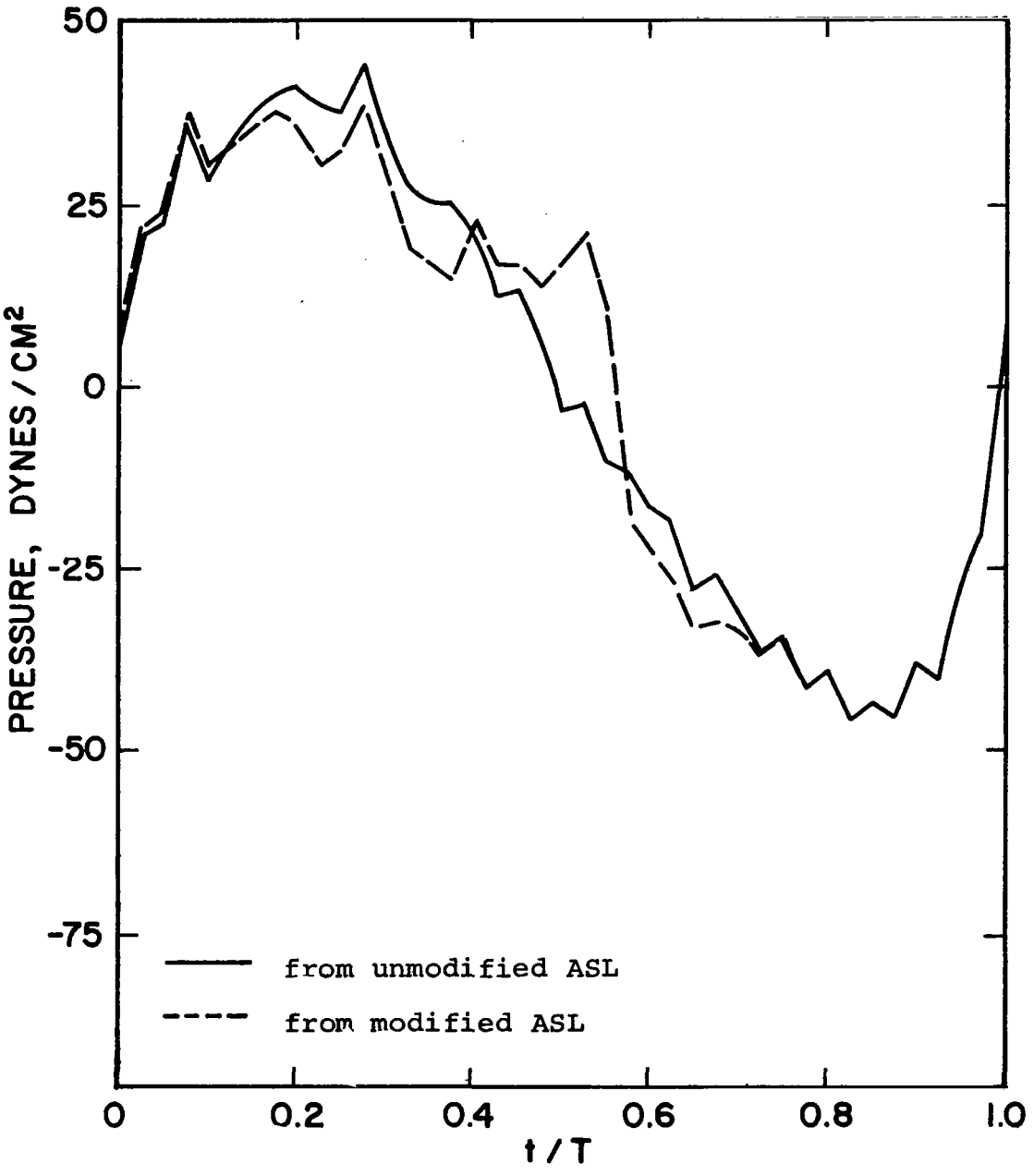

Figure 23. Comparison of computed pressure time histories from unmodified and from modified ASL's for H-34 helicopter. Rotational noise only, V=115 knots, F.P. 4.

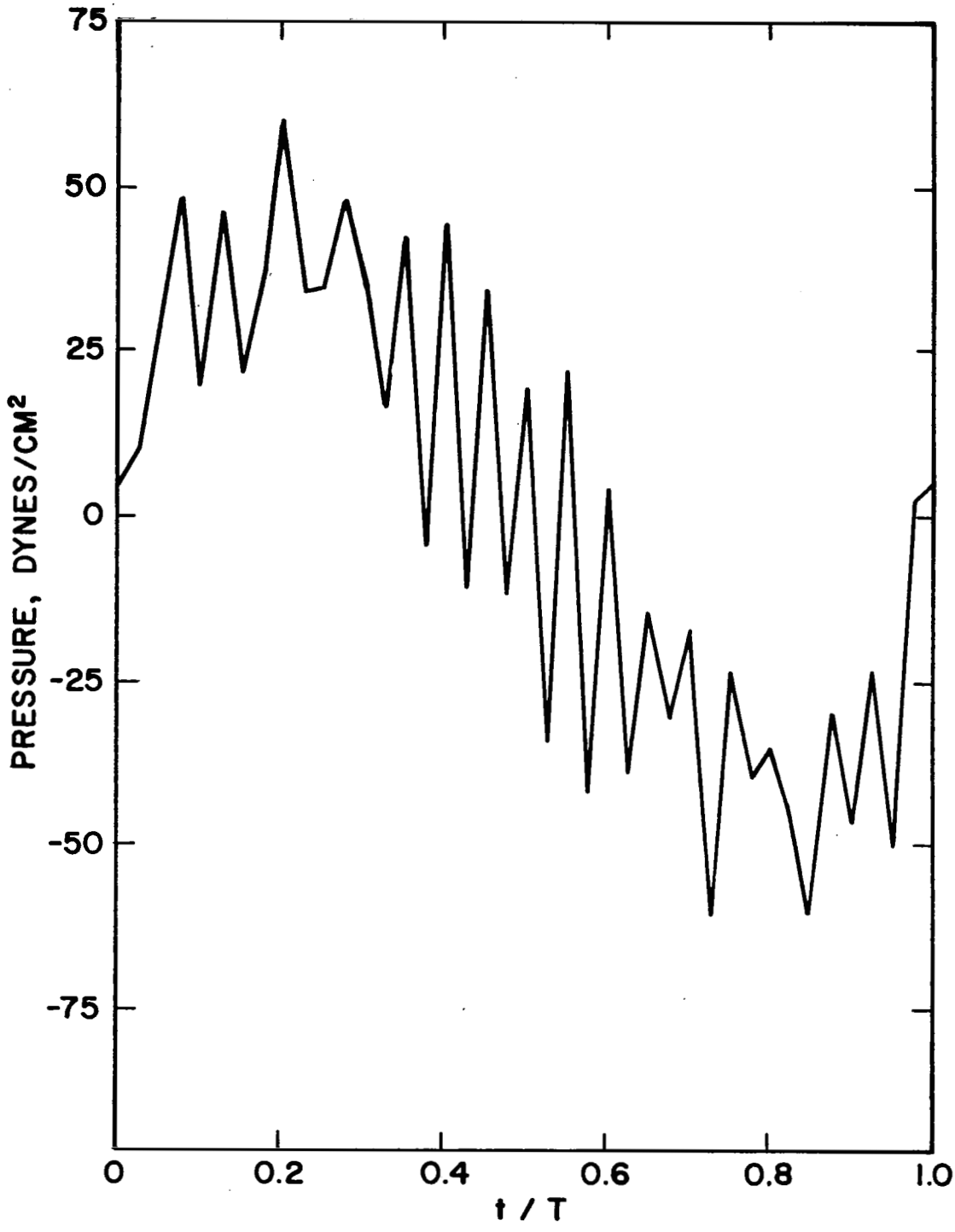

Figure 24. Computed pressure time history from unmodified ASL's for H-34 helicopter. K_L=1.0, K_D=0.5, V=115 knots, F.P. 4.

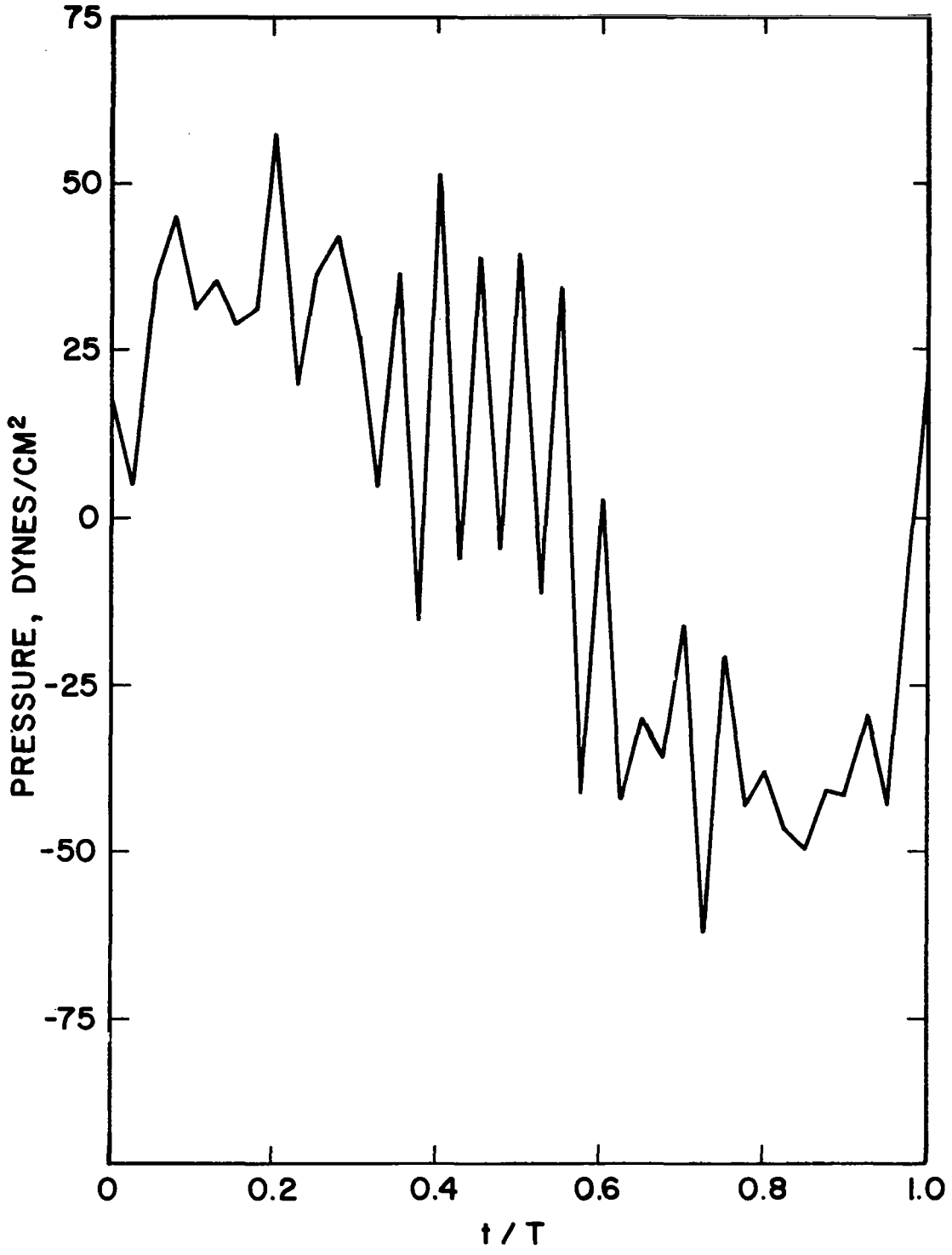

Figure 25. Computed pressure time history from modified ASL's for H-34 helicopter. K_L=1.0, K_D=0.5, V=115 knots, F.P. 4.

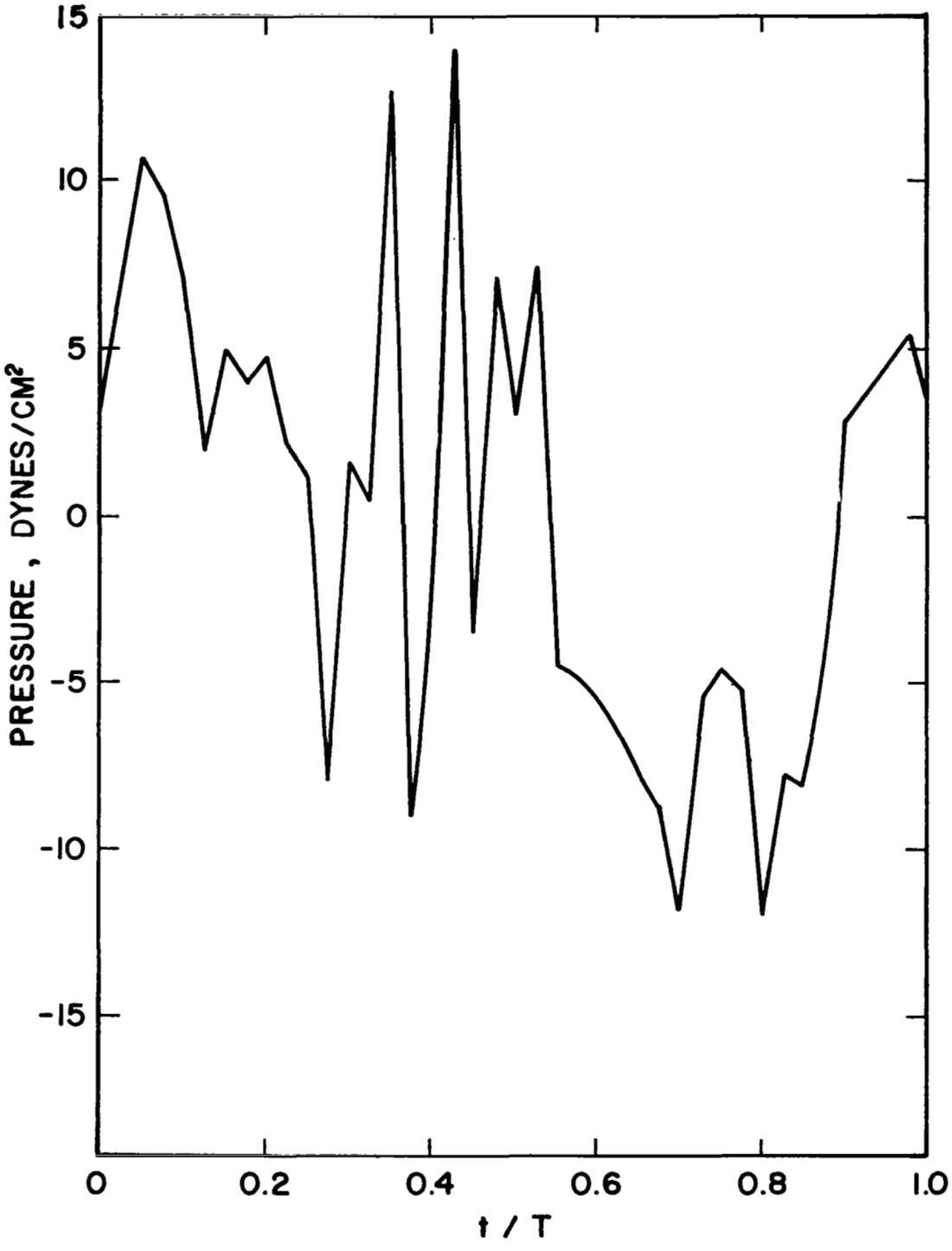

Figure 26. Computed pressure time history from steep descent ASL's for H-34 helicopter. K_L=1.0, K_D=0.5, $\bar{V} \approx 0$, F.P. 4.